Physics – Uspekhi **64** (9) 861 – 889 (2021)

REVIEWS OF TOPICAL PROBLEMS PACS number: **95.35.+d**

Search for weakly interacting massive dark matter particles: state of the art and prospects

A B Aleksandrov, A B Dashkina, N S Konovalova, N M Okat'eva, N G Polukhina, N I Starkov, V E Tioukov, M M Chernyavsky, T V Shchedrina

DOI: https://doi.org/10.3367/UFNe.2020.11.038872

Contents

Abstract. Determining the nature of dark matter (DM) is one of the most important challenges of modern experimental physics. This article overviews the major arguments confirming the existence of DM, gives the latest classifications of DM particles, identifies possible candidates for their role, and discusses the most significant DM particle search experiments conducted and under development. The article mainly aims to give an idea of diverse experimental methods of and approaches to registering DM particles, as well as of the currently available results of the search for them, which open new prospects in DM studies and contribute to solving topical problems in New Physics.

Keywords: dark matter, cosmic rays, direct and indirect search for dark matter particles

1. Introduction

Astronomical observations of the motion of galaxies and cosmic microwave background radiation show that a major part of matter in the Universe is not visible. According to current views [1], no less than a quarter of matter in the cosmos (so-called dark matter, DM) does not interact with electromagnetic radiation (does not emit, absorb, or dissipate it) and does not emanate any other known radiation of sufficient intensity, which prevents its detection by the existing methods of modern physics.

Analysis of astronomical data when the observed phenomena do not obey the laws of classical celestial mechanics had already led to the discovery of earlier unknown material space objects (the planet Neptune [2], the star Sirius B [3]) and continues to generate new hypotheses. One such indirectly confirmed hypothesis is the existence of DM. Evidence of its gravitational impact on other space objects is proof that it does exist. Numerous experimentally observed phenomena, from the expansion of the Universe to the motion of stars in galaxies, cannot be explained by the presence of exclusively visible matter. The statement of these facts led to the emergence of the theory of undetectable DM and the idea that galaxies are incorporated into its spherical halo (see, e.g., [4, 5]).

The concept of DM gained ground close to one hundred years ago after the publication of studies by Fritz Zwicky, who found that, for the Coma cluster of galaxies to be stable, it is necessary that its total mass exceed tens of times the combined masses of stars in it [6]. Since that time, a sufficient body of experimental evidence for the existence of a hidden mass in the Universe (the orbital velocities of stars in the gravitational fields of galaxies, gravitational lensing on galactic clusters, etc.) has emerged to enable establishing the fact of its existence and localizing regions of its clustering but providing no information about what it consists of.

Dark matter is, apparently, formed by an absolutely new type of stable particle, which has a nonzero mass (is involved in gravitational interactions with baryonic matter) and can presumably undergo weak interactions [7]. The possibility of weak interactions gives hope for a direct registration of DM particles in their interactions with atomic nuclei of baryonic

A B Aleksandrov [(1,2,3,a)], **A B Dashkina** [(3,b)], **N S Konovalova** [(1,3,c)], **N M Okat'eva** [(1,3,d)], **N G Polukhina** [(1,3,4,e)], **N I Starkov** [(1,3,f)], **V E Tioukov** [(1,2,g)], **M M Chernyavsky** [(1,h)], **T V Shchedrina** [(1,3,i)]
[(1)] Lebedev Physical Institute, Russian Academy of Sciences, Leninskii prosp. 53, 119991 Moscow, Russian Federation
[(2)] INFN — National Institute of Nuclear Physics, Sezione di Napoli, via Cintia 1, 80126 Napoli, Italy
[(3)] National University of Science and Technology MISIS, Leninskii prosp. 4, 119049 Moscow, Russian Federation
[(4)] National Research Nuclear University MEPhI, Kashirskoe shosse 31, 115409 Moscow, Russian Federation
E-mail: [(a)] andrey.alexandrov@na.infn.it, [(b)] asmailovab@gmail.com, [(c)] ninakonovalova@yandex.ru, [(d)] natalya_okateva@mail.ru, [(e)] polukhinang@lebedev.ru, [(f)] starkovni@lebedev.ru, [(g)] valeri@na.infn.it, [(h)] mmchernyav@yandex.ru, [(i)] tvshchedrina@gmail.com

Received 28 May 2020, revised 13 November 2020
Uspekhi Fizicheskikh Nauk **191** (9) 905 – 936 (2021)
Translated by V D Selivanov

matter. Hypothetical particles that could form DM are mainly the subject of theories beyond the Standard Model (SM). The nature of DM carriers is at present one of the major unsolved problems of modern cosmology, and the search for methods to register them is stimulating the development of new methods of experimental physics.

Experiments on the search for DM are conducted in three areas: the search for the interaction of DM particles with baryonic matter in laboratory experiments (direct registration), the search for products of DM annihilation or decay in outer space (indirect registration), and the production of DM particles in accelerators. Experiments on accelerators are discussed in detail in, for example, a review [8]. The present review deals with modern approaches to the search for signals from DM particles by their direct and indirect registration.

Section 2 discusses available evidence for the existence of DM. Section 3 reports on putative DM carriers. Section 4, as exemplified by a number of the most promising experiments, gives a brief overview of some major experimental spheres in the direct and indirect search for DM particles.

2. Available evidence for the existence of dark matter

Numerous indirect manifestations of DM have been registered by various astrophysical methods (see, e.g., [9]). Some experimental evidence for the existence of DM is given below.

Orbital velocities of stars in the gravitational field of galaxies. The most convincing and direct pieces of evidence for the existence of DM were obtained from observations of the rotation curves of spiral galaxies, i.e., the dependences of the orbital velocities of stars and gas on their distances to the center of a galaxy.

According to the virial theorem, mass $M(r)$ at distance r from the center of a galaxy is related to its rotation velocity as

$$M(r) \propto \frac{V^2 r}{G_{\mathrm{N}}}\,, \tag{1}$$

where G_{N} is the gravitational constant.

The rotation velocity V is measured by observing emission lines HI (neutral hydrogen; the wavelength without taking into account the Doppler effect, 21 cm) beyond the visible part of a galaxy.

If the visible mass of a galaxy were its main mass, $M(r)$ beyond its limits should be constant, and the orbital velocity of the galaxy, as per Kepler's third law, should decrease as $V(r) \sim r^{-1/2}$. However, the measured rotation velocities for the investigated galaxies proves constant at large distances in the direction to the limb of visible disks and independent of the distance to the center of the galaxy [10] (Fig. 1). This means that the main mass is beyond the visible part of the galaxy. Measurements of the rotation velocities in elliptic galaxies also show the presence of invisible matter [11].

Experimental data obtained in both the optical [13] and radio [14] ranges indicate that all observed galaxies are enclosed in a DM halo, which extends beyond the limits of their visible diameter. Thus, according to estimates, 95% of the Milky Way galaxy consists of DM [15].

X-Ray emission from hot gas in elliptical galaxies is also an important piece of evidence for the existence of DM. Detailed profiles of hot gas temperature and density for large elliptical galaxy M87 were drawn up by registering X-ray emission [16]. These measurements enabled determining the distribution of masses in the galaxy, required to bind hot gas while taking into account the hydrostatic equilibrium. The authors of [17] have shown that the total mass at a radial distance of 392 kpc is $5.7 \times 10^{13} M_{\odot}$, whereas the mass in a hot gas does not exceed $2.8 \times 10^{12} M_{\odot}$, or 5% of the total mass, and the visible mass, about 1%. M87 is not the only example of an elliptical galaxy, where X-ray emission from hot gas points to the presence of DM. Similar conclusions regarding the existence of DM were made from the X-ray emission from small groups of galaxies [18].

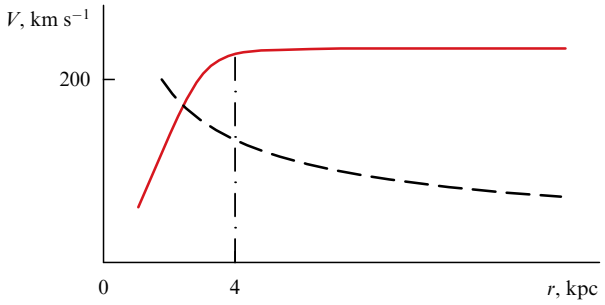

Figure 1. Orbital velocities of stars around the centre of a spiral galaxy. The dashed line shows a decrease in velocities for the Kepler orbits depending on distance r from the spiral galaxy centre. The solid line shows a rotation curve obtained by the averaged experimental data. (From [12].)

One of the strongest arguments in favor of the existence of DM is *gravitational lensing*. The presence of DM is detected by analyzing how its gravitation affects the distribution of light from remote galaxies. Clusters of galaxies contain the strongest gravitational potential in the Universe; for this reason, they are of greatest interest from the viewpoint of gravitational lensing effects. Distortions produced on images of remote background galaxies by these clusters can be used to reconstruct distributions of masses where DM is assumed to significantly predominate. The map of distorted light created by gravitational lensing enables tracing how DM is distributed in a galactic cluster. The obtained masses of galaxy clusters significantly exceed the mass of luminous matter [19].

This is how the ring of DM around the center of the galaxy cluster Cl0024+17 was found. A study analyzing the distortion of light from background galaxies by this cluster was carried out based on data from the Hubble Space Telescope observatory registering electromagnetic emission within the range from ultraviolet to infrared [20]. Blue bands in the central part of the image in Fig. 2 are strongly lensed objects representing smeared images of extremely distant galaxies that are not part of the cluster. The shapes of these galaxies are distorted, because their light is bent by the powerful gravity of Cl0024+17.

Strongly lensed objects severely limit the mass structure of the cluster's inner region. A reconstruction of Cl0024+17 mass distribution obtained in this way shows a ring-like substructure of DM enclosing the dense core of the cluster. Computer simulation enabled localizing the ring-like DM region by superimposing it on a digitized image of Cl0024+17 (see Fig. 2) and assessing the outer radius of this ring as ~ 0.4 Mpc. The discovery of the ring is one of the most convincing indirect pieces of evidence for the existence of DM.

Results from the Planck satellite show that DM makes up 83% of the density of matter in the Universe [22], and one of the major issues today is the nature of particles that form DM.

Figure 2. (Color online.) Image of the Cl0024 + 17 galaxy cluster taken by the Hubble Space Telescope was overlaid by a reconstructed map of the DM 'ring' around the cluster centre (composite image from [21]).

3. Putative carriers of dark matter

At present, there are a large number of theoretical models for describing candidate DM particles. These models have been rapidly developed, expanded, and supplemented with new details, and it is impossible to describe all of their diversity in a short review. Here, we present only the most essential theoretical hypotheses about classes of DM particles.

The relative number of different types of matter is usually presented as Ω, the ratio of the average density of a certain type of energy to critical density $\rho_c = 3H/(8\pi G_N) = 0.85\times 10^{-29}$ g cm^{-3}, where $H = 67.3$ km s^{-1} Mpc^{-1} is the Hubble constant. The values of these magnitudes measured in cosmological studies are [22] $\Omega_{BM} = 4.9 \pm 0.0016\%$ for baryonic matter, $\Omega_{DM} = 26.8 \pm 0.014\%$ for dark matter, and $\Omega_{DE} = 68.3 \pm 0.015\%$ for dark energy. The total density Ω_{tot} is very close to unity, which means that the four-dimensional pseudo-Euclidean spacetime of our Universe is flat, and the three-dimensional space is almost Cartesian.

Most evidence for the existence of DM is based on gravitational interactions. However, baryons are captured into gravitational wells of dark matter concentrations and, though DM particles themselves are not involved in electromagnetic interactions, congregations of dark substance in the cosmos are observed have emissions within a wide range of frequencies and energies (see Section 4.1.1). The property of gravitational instability makes it possible to investigate the amounts, states, and distributions of DM by observational data within the range from radio to X-ray emission.

It is considered that the properties of DM carriers (their mass, features of interaction between themselves and with other particles) should be consistent with models for the evolution of the Universe and with the Standard Model of elementary particles, which satisfactorily describes most physical data observed. If particular types of DM that emerged as the result of the Big Bang are stable, they can occur in the present-day Universe as relic particles.

Factual information about the properties of objects that make up DM is extremely scarce. As such objects form the bulk of galaxies, they should therefore possess nonzero masses. The theoretical spectrum of masses for the discussed candidates is very wide and extends from values of the order of 10^{-21} eV (the de Broglie length of the central part of a dwarf galaxy) [23] to 10^{19} GeV (the Planck mass) [24]. Moreover, as these particles have survived from the moment of the Big Bang till now, their lifetimes should be very large; most models assume them to be stable. Furthermore, as DM particles are not essentially involved in electromagnetic interactions, they should be electrically neutral, though some models allow a small charge $q_{DM} < 10^{-3}e$ in them [25].

The most actively discussed candidates are weakly interacting massive particles (WIMPs), which experience a gravitational interaction and interact with W and Z bosons of the SM. Theoretical arguments in favor of choosing WIMPs as DM particles consist in the possibility of describing a plausible scenario for the evolution of the Universe and, at the same time, to reconcile their properties to the SM.

In the early Universe, DM particles were in equilibrium with the other types of matter. Then, as the Universe expanded and cooled, the density of DM began to drop, with temperature T changing in accordance with the law $n_X \propto \exp(-m_X/T)$, where m_X is the mass of DM particles. At temperature $T < m_X$, dark matter freezes out, and its density decreases so much that interactions of individual DM particles become very rare, and their annihilation processes weakly affect their total number. As a result, DM forms relic radiation whose density asymptotically approaches some equilibrium value determined by the ratio of the reaction rates of annihilation of DM particles (XX) into common SM particles (XX $\rightarrow$ SM) and the reverse reaction (SM $\rightarrow$ XX). To realize this scenario, it is required to have an optimal ratio between the WIMP annihilation reaction rate proportional to the value of $n_X\langle\sigma_{XX}v\rangle$ (where v is the velocity of particles, $\langle\sigma_{XX}v\rangle$ is the velocity-averaged cross section of the reaction, n_X is the density of particles) and the Universe expansion tempo determined by the Hubble constant H. Consideration of this scenario for the evolution of the Universe [26] leads to the ratio

$$\Omega_X H^2 \propto \frac{1}{\langle\sigma_{XX}v\rangle}\,. \qquad (2)$$

If it is assumed that $\Omega_X = \Omega_{DM}$, this relation leads to a cross section value of the order of a picobarn (10^{-36} cm^2), which is in agreement with the hypothesis of the involvement of WIMPs in a weak interaction. The cross section $\Omega_X = \Omega_{DM}$ corresponds to the relation $\langle\sigma_{DM}v\rangle$.

The fraction of DM for WIMPs depends on the cross section of annihilation of its particles, which is related to the mass. It turns out that particles having masses within the limits of $m_X \sim 30-300$ GeV may be responsible for 10% of Ω_{DM}, whereas particles with masses within $m_X \sim 100$ GeV–1 TeV can describe the entire Ω_{DM} [27]. In this respect, WIMPs are very 'convenient', because they enable a flexible regulation of their contribution, bringing this value into line with the Universe's evolution scenario starting from the moment of the Big Bang. Figure 3 [26] presents a semiquantitative dependence of particle density Y and energy density Ω_X on time and temperature for WIMPs with masses of 100 GeV. Curves *1*, *2*, and *3* correspond to values of $0.01\langle\sigma_{XX}v\rangle$, $\langle\sigma_{XX}v\rangle$, and $100\langle\sigma_{XX}v\rangle$.

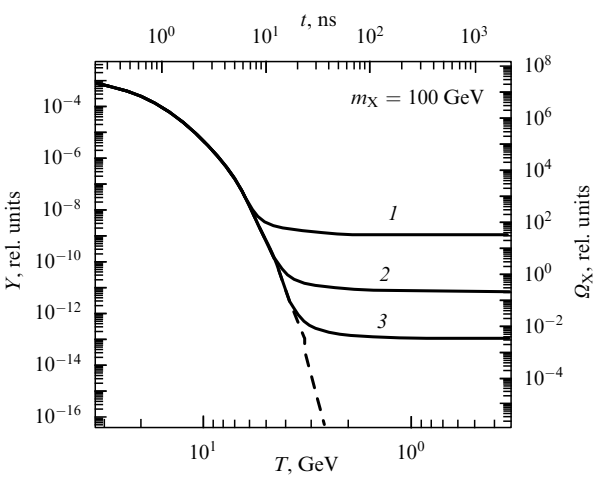

Figure 3. Semiquantitative pattern of the evolution of the Universe for the case of WIMP particles with masses of 100 GeV. Dependence of particle density Y and energy density Ω_X on time t and temperature T is shown. Curves *1*, *2*, and *3* correspond to values $0.01\langle\sigma_{XX}v\rangle$, $\langle\sigma_{XX}v\rangle$, and $100\langle\sigma_{XX}v\rangle$. (From [26].)

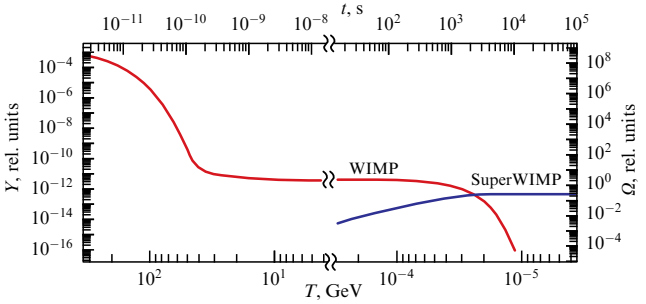

Figure 4. Change in particle density Y and energy density Ω as a function of time t and temperature T [34].

WIMPs can be detected by their annihilation products, e.g., by a pair of neutrinos. If a WIMP possesses a sufficiently large mass, a decay into two or more particles is possible.

The main candidates for the role of WIMPs are neutralinos, the lightest supersymmetric particles, which are a combination of calibration-boson superpartners. The range of their masses is estimated to be within 30 GeV $< m_X <$ 5 TeV. They are searched for in acceleration experiments that impose additional restrictions on the mass [28].

Other possible WIMP candidates are particles emerging in theories with extra Kaluza–Klein-type dimensions [29]. There are several theories of this type, which include particles that can be considered for the role of DM, in particular, unified extra dimension theories [30]. Estimates for m_X within the range from 400 to 1200 GeV were obtained for the masses of the lightest of them [31].

Yet another class of particles for the role of DM are SuperWIMPs, which interact much more weakly than in the case of the usual weak interaction. In the evolution of the Universe, they emerge at one of the last stages as the result of the decay of common WIMPs [32, 33]. The expansion of the Universe and the freeze-out of WIMPs initially proceed in this model by the usual scenario; SuperWIMPs weakly affect the process due to the smallness of interaction with them and, as a result, are not in equilibrium with WIMPs. At this stage, $\Omega_{WIMP} \sim \Omega_{DM}$. If it is assumed that each WIMP decays into one SuperWIMP and their masses are close, the density of relic SuperWIMPs will be of the order of Ω_{DM}, whereas that of WIMPs will be small.

Figure 4 schematically presents a density change pattern for particles Y and energy Ω as a function of time t and temperature T [34]. An advantage of this pattern is that WIMPs involved in the evolution mainly at only the early stages are not bound by the limitations on their properties required for DM. For instance, they can be charged. Gravitinos in supersymmetric theories and gravitons in theories of extra dimensions are considered candidates for the role of SuperWIMPs.

One of the most natural hypotheses regarding the nature of DM is an assumption of the existence of baryonic macroscopic astronomical objects given the name Massive Astrophysical Compact Halo Objects (MACHOs) (see, e.g., [35]). These can be compact star-like objects (neutron stars, brown dwarfs, etc.) or Jupiter-type planets, as well as primordial black holes. MACHOs can be found, for example, in gravitational lensing experiments. On the other hand, if all DM is represented by baryons, then the concentration ratio of light elements after primordial nucleosynthesis observed in most old astronomical objects should be different, sharply differing from that observed. Moreover, experiments searching for gravitational lensing of the light from our Galaxy's stars show that no sufficiently high concentration of large gravitating objects like planets or black holes is observed to explain the mass of our Galaxy's halo, and small objects should absorb the light of stars too strongly. Nevertheless, MACHO and EROS (Environmental Reward Observation Scale) experiments [36] monitored stars in the Small and Large Magellanic Clouds, from the results of which an estimated total mass of MACHOs in the galactic halo was less than 15% of the halo mass.

Particles possessing appropriate properties have been described in quite a number of theories and have been searched for in most diverse experiments for many years now. Common SM neutrinos can be mentioned among the most known particles that satisfy the required properties for DM carriers. However, existing estimates of the upper limit of the total mass of three types of neutrinos and energy density ($\Omega_\nu \approx 0.3\%$) show that their contribution to DM is too small to completely describe the observed magnitudes, though some proportion of neutrinos in DM is probable.

The discovery of neutrino oscillations is indicative of their masses (see, e.g., [37]). In the Standard Model, they are massless, so the need to expand the SM is evident. One of the variants of such an expansion is the introduction of a sterile neutrino [38]. In this case, right-handed sterile neutrinos, which do not interact with W and Z bosons and cannot be registered in experiments directly, are added to the left-handed neutrinos of the Standard Model. Their link with common neutrinos is by way of mixing; the mixing angle should be rather small. In this case, sterile neutrinos should decay into common neutrinos to form photons. Furthermore, their masses should be sufficiently high for them to be able to smooth fluctuations of matter in the Universe on smaller scales than their path lengths and, thus, to satisfy the constraints that follow from observations of the large-scale structure of the Universe [39]. There is a contradiction in the assessments of sterile neutrinos' characteristics. Thus, in the assumption of certain models for the formation of sterile neutrinos in the early Universe, paper [40] obtained a constraint for the mass of a sterile neutrino at $m_{ster} \geqslant 14$ keV, whereas in [41] it was

estimated as $m_{\text{ster}} \sim 10$ keV. For other mechanisms, the constraints are weaker.

Another class of possible candidates for DM are particles of the so-called hidden sector, which do not interact with SM particles straightforwardly and cannot be registered in an experiment directly. Their coupling with Standard Model sector particles is via an intermediary particle. Several models of such a coupling are considered, where, for instance, the neutrino [42] or the Higgs boson [43] serve as a mediator.

By way of example, consider in more detail the dark photon [44], which is introduced through so-called kinetic mixing. For this, the theory considers an additional calibration group $\mathrm{U}(1)'$, and the interaction of the massive dark photon A'_μ with the regular electromagnetic field is described in this case by a Lagrangian

$$L = L_{\text{SM}} - \frac{1}{4}\,(F'_{\mu\sigma})^2 + \frac{\epsilon}{2} F'_{\mu\sigma} F^{\mu\sigma} + \frac{m^2_{A'}}{2} A'_\mu A'^{\mu}\,, \qquad (3)$$

where L_{SM} is an SM Lagrangian, A'_μ is a massive calibration field, $F'_{\mu\sigma} = \partial_\mu A'_\sigma - \partial_\sigma A'_\mu$, and ϵ is the kinetic mixing parameter. In this variant of the theory, the dark photon interacts with massive Dirac particles of dark matter X:

$$L_{\text{X},A'} = -\frac{1}{4}\,(F'_{\mu\sigma})^2 + \bar{X}\left[\gamma_\mu(\mathrm{i}\partial_\mu - g' A'_\mu) - m_{\text{X}}\right] X\,, \qquad (4)$$

where g' is the 'charge' of particles X in the new calibration group. Variants of the complex scalar field X are also considered. Theoretical and experimental estimates of the magnitudes of ϵ and g' yield small values; nevertheless, the dark photon can manifest itself in experiments where a sufficiently energetic common photon emerges: the decay of neutral pions, bremsstrahlung, the elastic scattering of charged particles, etc.

Yet another candidate for DM is the axion, a particle introduced into the theory to solve the problem of the absence of charge parity (CP) violation in strong interactions [45], i.e., the existence of an invariance relative to a combination of charge conjugation (C) and parity (P) in strong interactions, in contrast to weak interactions, where this invariance is violated. On the other hand, vector currents present in the QCD Lagrangian allow CP violation. One of the violation features is the neutron electric dipole moment. Theory estimates it to be $d_{\text{e}} \sim 10^{-16} e$ [cm]. At the same time, experiments yield a clear-cut limit of $d_{\text{e}} < 10^{-26} e$ [cm], which is 10 orders of magnitude lower than the expected value. To explain the absence of CP violation in the SM, an additional pseudoscalar field and axions (particles corresponding to it) are introduced. The masses of these particles and their interaction constant are very small. Usually, when discussing axion masses, m_{a}, use is made of a model-dependent expression relating the mass of an axion and the constant of its decay into two photons, f_{a} [46]:

$$m_{\text{a}} = 6\left(\frac{10^9\ \text{GeV}}{f_{\text{a}}}\right)[\text{meV}]\,.$$

Notably, the Planck experiment found the upper limit of the axion mass to be $m_{\text{a}} < 0.67$ eV at a 97% confidence level [47] and a total neutrino mass constraint of $\Sigma m_\nu < 0.7$ eV, which is related to the constant f_{a}. The treatment of the data for the supernova 1987A explosion leads to a more stringent constraint on the mass: $f_{\text{a}} \geqslant 4 \times 10^8$ GeV, $m_{\text{a}} \leqslant 16$ meV [48].

From the viewpoint of the behavior of DM at the initial stages of evolution of the Universe, it is divided into hot, warm, and cold, depending on the stage of its particles' freeze-out, namely, the particles' mean path lengths as compared to the scale of the Hubble expansion of the Universe. The current scenario for the formation of galaxies and other cosmic structures is based on their origination due to a gravitational collapse of DM density inhomogeneities reaching sufficient magnitudes. The most suitable candidate in the description of this process is cold DM, the concept of which had earlier demonstrated its potential by predicting the anisotropy of relic radiation. Particles of this type of DM decoupled from cosmic plasma, being already nonrelativistic. Their use enables a good description of the observed cosmological data and the large-scale structure of the Universe on a scale of masses $> 10^{10} M_\odot$. WIMPs and axions are considered candidates for cold DM particles. However, the characteristics of smaller structures that emerge in this approach are in contradiction with a number of modern observations. In particular, far too large a number of galactic satellites is predicted as compared with the observed satellite galaxies.

Moreover, for cold DM particles the so-called singular halo problem exists, emerging from numerical simulations of DM distribution [49]. Calculations unambiguously indicate that cold DM would form a cusp, or a singularity (a sharp peak in the distribution), in the center of the galaxy or, on the whole, in denser regions of the Universe far stronger than in its other regions. However, all direct astronomical observations that led to the finding of the DM effect show an opposite picture: DM forms a halo around galaxies by filling voids between galactic clusters and shows no singularities (cusps) in its distribution.

Introducing warm DM into consideration helps to improve the description of small-scale structures of the Universe. Its particles left the equilibrium being ultra-relativistic but became nonrelativistic (critical velocity of $\sim 0.001c$) by the moment of transition to a dust-like stage of development. The number of small-mass objects formed by warm DM is much fewer than in the case of cold DM, which decreases the discrepancy between theory and experiment. Sterile neutrinos [50] or light gravitinos [51] could act as warm DM particles.

Hot DM includes particles that move at ultra-relativistic velocities. Due to enormous velocities, these particles are not capable of forming stable structures but can affect common matter and other kinds of DM. High velocities lead to a disruption of density perturbations, thereby preventing the emergence of large-scale structures of the Universe, which contradicts observations; therefore, hot DM cannot be too much. Only very light particles like common neutrinos can be hot DM particles.

There are other variants of DM particles apart from the examples presented, e.g., the magnetic monopole, the cosmion, etc., not considered here. Furthermore, models not associated with particles have been proposed, a sort of gravity in theories of extra dimensions relating visible matter from our measurements to massive matter from other measurements, which may lead to the effect of DM. Or else DM may be original defects of space or quantum-field topology emerging at the moment of the Big Bang. They may contain energy, evoking gravitational forces.

4. Experimental methods in the search for dark matter particles

The experimental search for putative DM carriers requires original approaches and immensely complex engineering

solutions (see, e.g., [52, 53]). New ideas and projects constantly emerge, which makes the situation rather dynamic. This section describes some — but far from all — of the most interesting and promising attempts currently in operation to register signals from DM particles.

4.1 Indirect registration of dark matter particles

DM carriers have a nonzero probability of annihilating or decaying to form SM particles (gamma quanta, neutrinos, electrons, positrons, and other cosmic ray (CR) particles) (see, e.g., [54, 55]).

For this reason, the search for signals from DM is possible by way of studying gamma radiation, fluxes of neutrinos, and charged high-energy CR particles. These particles, however, can also form as a result of common astrophysical processes. As DM particles have quite certain (but yet unknown) masses, products of their direct annihilation should have narrow linear characteristics, i.e., products of decay or secondary particles of annihilation shall be distributed within a certain energy range. Indirect detection of DM consists in the search for particular features in the energy spectra of cosmic rays and anomalies in the expected background spectrum of known astrophysical processes [56]. The vast majority of indirect experiments, both implemented and scheduled, is aimed at searching for signals from WIMPs as the most probable candidates of DM carriers.

4.1.1 Registration of the electromagnetic component of cosmic radiation. It is expected that heavy particles of cold DM can annihilate or decay to form gamma quanta having, depending on the reaction channel, continuous-energy or monoenergetic spectra. Gamma radiation is an extremely promising object for the indirect detection of DM, because it is not deflected by magnetic fields and yields to registration more readily than neutrinos.

Gamma quanta with strictly defined energies equal to the masses of sought-after particles should emerge in the annihilation of WIMPs. On the gamma radiation spectrum, this should lead to the emergence of a peak at a corresponding wavelength. The flux of gamma quanta originating upon the annihilation of DM particles is determined by the cross section of the process and the masses of particles, as well as by the distribution of matter inside the halo. By studying fluxes of excessive gamma quanta, one may obtain a constraint for the annihilation cross section for hypothetical particles with masses from 10 to 10^4 GeV [57]. At a small flux of excessive gamma radiation, the constraint are very rigid.

Spectral lines are some of the most powerful signatures in the search for DM annihilation in very-high-energy γ-rays. At the same time, the monochromatic signal from the annihilation into photons is suppressed compared with the other channels, because DM particles do not carry electric charges.

The center of our Galaxy is the brightest of the sources of observed (from the Earth) high-energy gamma radiation presumably caused by the annihilation or decay of DM particles [58]. As Earth's atmosphere is opaque to cosmic gamma radiation, the detection of gamma quanta from DM particles is possible only in outer space using space-based gamma telescopes.

Study [59] determined the values of gamma-radiation detector energy resolution required to register signals from WIMPs. It has been shown that, while a resolution of $\sim 10\%$ is sufficient to register formed gamma quanta with continuous energy spectra, the registration of monoenergetic lines requires a resolution of less than 5%.

Galactic diffuse high-energy gamma radiation was registered in several experiments; however, the most significant results, from the viewpoint of DM signal studies, were obtained using the Large Area Telescope (LAT) [60].

The wide field-of-view LAT telescope operated in the scanning mode (effective registration area of about 1 m^2; field of view of ~ 2.4 sr) is the primary instrument of the Fermi Gamma-ray Space Telescope (FGST) launched into near-Earth orbit in 2008 [61] and still functioning. The detector operates by the principle of registering electron-positron pairs formed during the passage of high-energy gamma rays through the detector volume (pair-production detector). The trajectories of formed electrons and positrons and their full energies are measured, which enables determining the direction and energy of the primary gamma quantum within the energy range from ~ 50 MeV to 1 TeV. The angular resolution of the telescope is 0.1°; the energy resolution is $\sim 10\%$.

Unique data about cosmic gamma emission have been obtained using the Fermi-LAT telescope; they include the detection of more than 5000 point-like gamma-ray sources [62]; excess emission from the Milky Way galactic center and from the Andromeda and Triangulum galaxies [63, 64]; Fermi bubbles [65]; as well as the assessment of the upper limit of the DM annihilation cross section [66].

Several years ago, the Fermi-LAT collaboration reported on the detection of a gamma-ray emission source in the Milky Way galactic center (GC) with quantum energy exceeding hard X-ray energy by two or three orders of magnitude. The gamma ray spectrum of the emission is consistent with the masses of DM particles from 10 GeV to 1 TeV annihilating into b and $\bar{b}$ quarks, and with masses from 10 GeV to 30 GeV annihilating into τ^+ and τ^- leptons (Fig. 5) [67].

Interpretation of these experimental data has been debated since their publication. Thus, an independent analysis of LAT data by research groups from the USA [69] and the Netherlands [70] in 2016 showed that the observed emission can be explained with high confidence by the emission of clusters of point-like sources with similar gamma-ray spectra, such as millisecond pulsars. Subsequently, these conclusions were refuted based on a new approach to the treatment of LAT data [71]; it has been shown that DM can, with high probability, be a dominant contribution to the excess gamma-ray emission of the GC. However, as the authors of the publication recognize themselves, their results are not the final proof for the existence of DM galactic halos.

The possibility of observing gamma-ray signals from smaller clusters of DM in the Galaxy, so-called subhalos, has also been considered [72]. However, as calculations have shown [73], the subhalo emission brightness does not exceed 10% of the ratio of the GC main halo brightness to the background, i.e., the registration of gamma-ray emission from DM subhalos by modern instruments has more uncertainties than that from GC halos.

Reliable identification of signals from DM in fluxes of cosmic electromagnetic radiation requires the use of equipment with a high angular, spatial, and energy resolution. The new-generation equipment is planned to be installed aboard the Russian astronomical satellite GAMMA-400 (Gamma Astronomical Multifunctional Modular Apparatus, with a maximum gamma-ray energy of 400 GeV) [74], which is

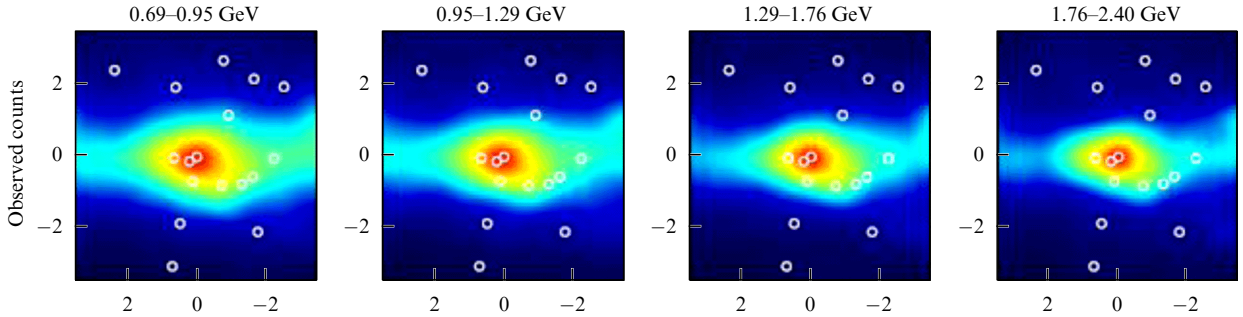

Figure 5. (Color online.) Map of excess diffuse gamma-ray emission in a $7^\circ \times 7^\circ$ region around the GC for four energy intervals of registered gamma quanta. LAT data [67]. Circles designate 17 unidentified point-like gamma-ray sources in the field of view from the 2FGL (Fermi Gamma-ray LAT) catalogue [68].

planned to be launched in 2026. The instruments installed on the satellite will register gamma quanta within the energy interval from 20 MeV to several TeV, and electrons (positrons) up to ~ 20 TeV. The angular ($\sim 0.01^\circ$) and energy ($\sim 1\%$) resolutions of the gamma telescope will exceed by 5- to 10-fold the corresponding parameters of both the Fermi-LAT and ground-based Cherenkov gamma telescopes, which will enable extracting more reliably possible signals from various DM particle annihilation channels.

Apart from galactic gamma radiation sources, of interest in the search for signals from DM is solar radiation [75]. It is assumed that DM particles from the galactic halo, when passing through the Sun and experiencing inelastic scattering on nuclei, lose their energy and are trapped by the gravitational field of the star. Accompanied by multiple scattering, these processes lead to a concentration of DM particles, simultaneously experiencing annihilation processes, inside the Sun [76]. Some annihilation models assume the formation of intermediate particles (mediators) capable of abandoning the Sun and decaying outside it into SM particles, e.g., gamma quanta and neutrinos [77, 78], which can be found by detectors on Earth or in a near-Earth orbit. According to other models, annihilation to form gamma quanta and electrons+positrons occurs without the involvement of the mediator particle [79].

Small by cosmic standards, the distance from Earth to the Sun enables registration of not only gamma quanta but also charged particles. Electrons and positrons formed as a result of DM annihilation should have a specific energy spectrum depending on the mechanism of their formation [80]. The expected signal should have a peak in the direction of the Sun, with an angular broadening determined by the heliospheric magnetic field.

A number of experiments, among which are those on the Fermi-LAT [81], PAMELA (Payload for Antimatter Matter Exploration and Light-nuclei Astrophysics) [82], and AMS-02 (Alpha Magnetic Spectrometer 02) [83] satellites, have found that the fraction of positrons in the total electron–positron flux increases within the energy interval from 10 GeV up to at least 250 GeV. These experimental data contradict the predictions of CR propagation models, according to which the fraction of positrons formed in the interaction of cosmic rays with interstellar gas should drop in this energy region [84, 85] (Fig. 6). The observed increase in the fraction of positrons can indicate that there is a source of these particles with high energies near Earth, and one of the possible mechanisms of their formation may be the annihilation or decay of DM particles [86].

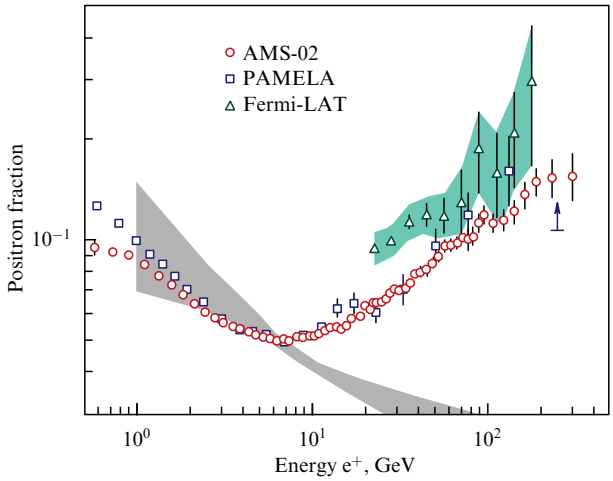

Figure 6. (Color online.) Anomalous exceedance of the fraction of high-energy positrons in cosmic rays. Data comparison of the AMS-02, PAMELA, and Fermi-LAT experiments with model calculations (grey area). (From [87].)

In this connection, of great interest are the results obtained in the DAMPE satellite experiment (DArk Matter Particle Explorer) registering cosmic electrons and gamma quanta within a broad energy range [88]. Using a combination of four subdetectors — a plastic scintillation strip detector, a silicon–tungsten tracker, a calorimeter, and a neutron detector — the DAMPE facility succeeded in very efficiently suppressing the cosmic-ray hadronic background and significantly improved energy resolution. The DAMPE satellite was put into a sun-synchronous orbit at an altitude of 500 km in December 2015. In total, about 1.5 million electrons and positrons with energies from 25 GeV to 4.5 TeV were registered whose spectra are described by a power law with the spectral index changing from ~ 3.1 to ~ 3.9 and a break in the region of 0.9 GeV (Fig. 7). It is expected that these results will help to elucidate the relation between the anomaly of positrons and the annihilation or decay of DM particles.

As the flux of cosmic gamma radiation rapidly decreases with increasing energy, observations at higher energies require instruments with a far greater effective registration area than in space-based telescopes. Ground-based Cherenkov gamma telescopes (Imaging Atmospheric Cherenkov telescopes, IACTs) register Cherenkov radiation generated by fluxes of particles induced in Earth's atmosphere by primary cosmic radiation (PCR), including high-energy electromagnetic radiation. It is evident that the effective

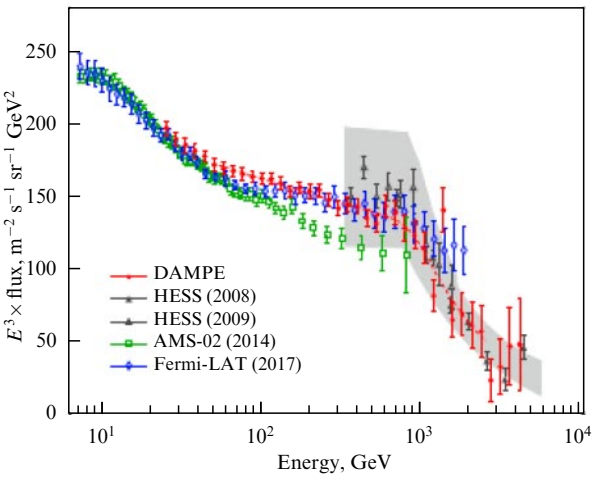

Figure 7. (Color online.) Total spectrum of cosmic-ray electrons and positrons ($\times E^3$) measured by the damping method in DAMPE, HESS (High Energy Stereoscopic System), AMS-02, and Fermi-LAT experiments. Dashed red line represents a power-law model, which corresponds in the best way to data within the energy range of 55 GeV to 2.63 TeV. Grey band shows a systematic error of the HESS experiment. (From [89].)

registration area of ground-based facilities noticeably (several-fold) exceeds the registration area of space-based telescopes. It is essential that IACTs make it possible to identify and reject with high efficiency cascades of particles initiated by PCR hadrons, considering only fluxes of particles from electrons (positrons) and gamma quanta. However, IACTs have far smaller observation angles, not more than 10°, which makes the requirements for their directionality stricter.

At present, four IACT facilities operate within the range from several ten GeV to 100 TeV and higher; as a result of their operation, the boundaries of DM particle masses and the upper limits of WIMP annihilation rates for various channels have been found. They are the gamma telescopes HESS [90, 91], MAGIC (Major Atmospheric Gamma Imaging Cherenkov Telescopes) [92], FACT (First G-APD Cherenkov Telescope) [93], and VERITAS (Very Energetic Radiation Imaging Telescope Array System) [94]. In 2018, the HESS group communicated the results of a ten-year-long search for the monoenergetic spectral line from annihilations of DM particles in the direction of the GC within the energy range from 300 GeV to 70 TeV using a two-dimensional maximum-likelihood method, which utilizes the advantages of both spectral and spatial features of the signal compared against the background [91]. As a result of the data treatment, no features of WIMP annihilation were found, but the currently most stringent constraints on the probability of this annihilation were obtained. The upper limit of the cross section of annihilation for DM monoenergetic lines was 4×10^{-28} cm^3 s^{-1} at a mass of 1 TeV.

New-generation Cherenkov gamma telescopes aimed at, among other aspects, searching for DM possess a substantially higher sensitivity than existing ones, which will enable them to search for signals from both WIMPs and axions (see, e.g., [95–97]).

4.1.2 Registration of neutrinos. Neutrinos having colossal free path lengths in most diverse media, save information about their energy spectra at birth, and directly indicate the source of their formation; this enables investigating most remote cosmic objects, including those inaccessible to gamma astrometry. However, the registration of these particles is associated with significant technological difficulties. Compensation for the smallness of the neutrino interaction cross section requires large-volume detectors well protected from the background of other particles.

Accumulating in astrophysical objects (including in the Sun and Earth) as a result of gravitational attraction, DM particles may annihilate to form neutrinos whose energies, according to estimates, exceed by several orders of magnitude those of neutrinos formed in nuclear reactions (several ten and hundreds of GeV vs. several MeV) [98]. For this reason, in observations, e.g., in the direction of the Sun or the center of Earth, DM annihilation products can be distinguished from the atmospheric neutrino background by their energies. Promising avenues for the search for neutrino signals from DM are, as in gamma astronomy, directions toward the center of our Galaxy and toward other galaxies and galactic clusters, because their observed gravitational masses significantly exceed the mass of the Sun. In that regard, the mean density of galactic matter is less than the solar density, and, due to a lesser scattering of DM particles on nuclei, higher-energy neutrinos than those from the Sun can be observed.

In 1960, M A Markov proposed the idea of setting up detectors to register 'astrophysical' neutrinos in deep lakes or in the ocean and to determine the directions of high-energy charged particles formed in their interactions using the produced Cherenkov radiation [99]. Using this approach, three tasks are solved: the compensation of small neutrino interaction cross sections due to the large mass of the detector, and a decrease in the background and the transparency of the medium for registering Cherenkov radiation. The basics of deep underwater neutrino detection started to be developed in Russia in the 1980s for an experiment in Lake Baikal, which is distinguished by a unique depth (more than 1 km in places), a high transparency of water, and seasonal icing, facilitating the delivery and installation of heavy instruments [100].

The currently used large detector volumes of underwater neutrino telescopes collect hundreds of neutrinos per day. They are open-type massive experimental facilities representing a system of Cherenkov counters and photomultipliers with a large number of registration channels mounted on vertical hawsers in water or in ice. The detectors register Cherenkov counts from relativistic muons and cascades of charged particles formed as a result of neutrino interactions within a radius of several kilometers from the facility. The atmospheric neutrino background is excluded by selecting events by their trajectories running in the bottom-up direction, i.e., corresponding to particles, products of interactions of high-energy 'astrophysical' neutrinos, that passed through the bulk of Earth. Sensitive to signals from all types of neutrinos within a broad range of energies, they search for DM in all possible annihilation channels. To scan the entire celestial sphere, the neutrino telescopes should be located in different hemispheres of Earth.

A large water Cherenkov neutrino telescope in the Northern Hemisphere, ANTARES (Astronomy with a Neutrino Telescope and Abyss environmental RESearch), with an effective registration volume of $\sim 10^7$ m^3 with respect to neutrinos with energies greater than 10 TeV, is located in the Mediterranean Sea; since 2008, it has been observing neutrino flux in the direction of the Southern Hemisphere [101]. The results of measurements by ANTARES have shown that, to achieve the required sensitivity to the flux of high-energy

neutrinos, the detector volume should be increased to at least 1 km^3. At present, the research infrastructure KM3NeT (Cubic Kilometre Neutrino Telescope) is being built in the Mediterranean Sea; it includes three sites with neutrino detectors (one of which is ANTARES) with a total effective volume of over 1 km^3. The construction of the facility is scheduled to be completed in 2025 [102].

The largest neutrino telescope built into ice is the IceCube neutrino observatory [103], which began data collection in 2010. The telescope, with a working volume of 1 km^3, was installed at the South Pole and equipped with detectors of Cherenkov radiation from particles generated in interactions of neutrinos moving through Earth in the direction from the North Pole. The neutrino telescope has an energy threshold of 100 GeV. A more densely instrumented core inside IceCube, called DeepCore [104], decreases the energy threshold to about 10 GeV, and the planned update PINGU (Precision IceCube Next Generation Upgrade) would reduce the threshold to several GeV [105], which would significantly expand the facility's potential in searching for signals from DM in the low-energy range. The data already obtained by IceCube enabled assessing neutrino fluxes from the Northern Hemisphere and from the Sun, to produce new constraints on the physical properties of DM particles and to refine the required sensitivity of neutrino telescopes registering 'astrophysical' neutrinos [106, 107]. The most significant contribution to neutrino astrophysics is IceCube's registration of several ten events from ultrahigh-energy neutrinos within the range $\geqslant 1$ PeV [108], which may be indicative of the existence of a peak of high-energy neutrinos, possibly from DM [109, 110] (Fig. 8).

In 2015, the first cluster of the Baikal-GVD (Gigaton Volume Detector) neutrino telescope was put into operation; the cluster comprises a module system of spatially separated photoreceivers, the distances between which coincide by their order of magnitude with the light absorption length. The photoreceivers are placed into glass spheres to protect them from external water pressure. The photoreceivers with electronic apparatuses required for their operation are fixed to vertical hawsers with a buoy on one end and an anchor on the other. The modular system with laser synchronization makes possible the further stage-by-stage expansion of the facility. Commissioning of the GVD-1 modification of the telescope with an effective volume of 0.4 km^3 is scheduled for 2020–2021. The final aim of the project is to develop a telescope of the order of a cubic kilometer, including about ten thousand light sensors [112].

The task of the Baikal-GVD facility is to single out cosmic sources of neutrinos, determine their locations in the sky, and, as far as possible, identify them with objects observed in the optical range. The equipment of the first cluster searched for a signal in the direction of the galaxy NGC 4993 where, as a result of a fusion of two neutron stars, a gravitational wave emerged, registered on 17 August 2017 by the LIGO (Laser Interferometer Gravitational-Wave Observatory) and Virgo detectors (event GW170817 [113]). The search for neutrino events in the direction of NGC 4993 by the Baikal-GVD telescope, conducted in the cascade mode in two different time intervals, yielded no expected results; however, it enabled determining the upper limits of the spectral fluence of neutrinos from this source.

Smaller-volume Cherenkov neutrino telescopes are placed in low-background underground laboratories (see Section 4.2.1). The largest of the underground neutrino

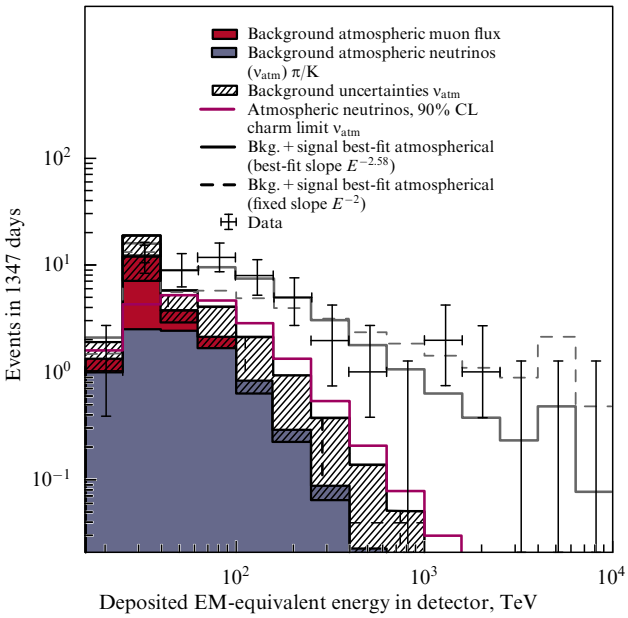

Figure 8. (Color online.) Energy distribution IceCube events, which can be interpreted as the occurrence of a peak at a level of about 2 PeV and a lower energy continuum separated by a dip slightly lower than 1 PeV [111].

telescopes in operation is the Super-Kamiokande facility [114], a water Cherenkov detector located at a depth of 1 km under Mount Ikenoyama (Japan), about 5×10^4 m^3 in volume. Over the observation period from 1996 to 2014, the experiment found no excess fluxes of neutrinos from putative sources of DM, such as the Sun, Earth, and the GC, compared with the expected atmospheric neutrino background within a broad neutrino energy range, with sensitivity to WIMP masses up to several ten GeV [115]. Possibly, this result is explained by a detector volume insufficient for observations of high-energy neutrinos. The volume of the new Hyper-Kamiokande detector, the construction of which is planned to start in 2020, will be 20 times larger [116].

Apart from Cherenkov neutrino telescopes, neutrinos from DM particles can be searched for by facilities based on scintillation and liquid argon detectors [117, 118], which represent a promising search direction in the field of low (GeV) energies.

The indirect discovery of DM particle annihilation and decay using observations of gamma quanta charged with cosmic rays and SM neutrinos appears to be a promising means for the identification of the nature of these particles. Significant success in both the set of data and their interpretation has been achieved over the past decade; taken together, they enabled establishing constraints on the physical parameters of DM particles and finding some intriguing hints for putative signals.

4.2 Direct registration of dark matter particles

Direct detection of DM particles is based on the registration of recoil nuclei upon the elastic scattering of WIMPs on target nuclei. As a result, energy within the range from 1 up to 100 keV is transferred to target nuclei, depending on the masses of the WIMPs and the features of interaction.

If in comparing the predicted frequency of events in the detector with the measured frequency the former proves to be greater, the registered particle with the corresponding event rate is ruled out as a DM candidate. However, the compar-

ison result of the expected signal with the experimentally observed spectrum cannot be sufficient proof of the registration of a WIMP, because this signal can be determined by background sources. Therefore, the sensitivity of the experiment in the selection of candidates and the limitation of their masses and interaction cross sections is determined by the level of the background. Additional evidence of the detection of a WIMP may be unique signatures characteristic of these events exclusively, which cannot be simulated by background or instrument effects. The only signature investigated to date is the annual modulation of the WIMP signal due to seasonal variations caused by the motion of Earth with respect to the Sun.

In 1988, Spergel pointed out that Earth's motion through the galactic halo of DM should cause a forward–backward asymmetry in recoil rates in the galactic system of coordinates [119]. The Solar System, moving in the galactic orbit, passes through the spherical halo of DM particles, which are considered to have a Maxwellian distribution of velocities [120, 121]. As a result, a directional flow of WIMPs relative to the Solar System emerges. Earth, in turn, moves around the Sun, which leads to annual fluctuations of the DM flow. The motion of the Solar System through the Galaxy causes a strong angular anisotropy in the distribution of WIMP velocities (in the coordinate system of Earth). The background distribution, in contrast, remains isotropic [122]. Variations in the DM particle flow caused by this relative motion are expressed in the modulation of the count rate of detectors that perform the direct registration of WIMPs. Expected event rates vary from one to less than 10^{-3} events per kilogram of detector material per year [123].

According to a widespread opinion, the anisotropy of the signal is the purest signature of galactic DM, insofar as none of the currently known sources of background events can simulate it. The literature describes several characteristics providing for an unambiguous discrimination between background events and WIMP scattering, e.g., the dipole structure [119], the ring structure (the maximum of the recoil rate lies on the ring around the mean recoil direction) [124], and aberration (the annual course of the mean recoil direction) [125]. Depending on the yet unknown cross section of WIMP–nucleon interaction, the registration of the recoil nuclear direction can be used for various purposes, such as the establishment of a stricter upper limit for the interaction cross section [126, 127], discovery of galactic DM [128–130], or investigation of the properties of WIMPs and local halos [131–134]. The use of information about the scattering direction would make it possible to achieve a sensitivity lower than the so-called 'neutrino limit' [135, 136].

A practically exponentially decaying energy spectrum of recoil nuclei makes the detection of WIMPs a rather complex experimental task. The low energy threshold of nuclear recoil detection and the small cross section of DM particle interaction with common matter determine the requirements for detectors and experimental conditions, such as a low background, a sufficiently large mass of the detector, and its stable long-time operation (about several years). Sections 4.2.1–4.2.7 present the major technologies used in direct experiments on the search for DM and review data summing up the main experimental results.

4.2.1 Underground laboratories for direct registration of dark matter particles. Due to the small cross section of interaction of DM particles with matter (the count rate of their detectors is estimated to be within the range from 10^{-6} to 1 events per kg per day [137]), experiments on their search by direct methods have one common feature: they are carried out in underground laboratories in order to significantly reduce the influence of the background. The high-energy background radiation affecting the radiopurity of measurements in these experiments is formed mainly by relativistic atmospheric muons and by the particles they induce. As at depths of over 200 m the muon flux attenuation is close to exponential [138], the background of relativistic particles in underground laboratories is significantly attenuated (Fig. 9), which provides a unique possibility for the search for rare events, such as WIMP scattering.

In particular, experiments on the direct search for DM particles are carried out in the following of the largest underground laboratories.

The China Jinping Underground Laboratory (CJPL) [139], located in the Jinping Mountains (China), is the deepest (2400 m of mountain rock or 6720 m water equivalent (w.e.)) and largest by volume (3×10^5 m^3). The muon flux in the laboratory space is a mere 2×10^{-6} m^{-2} s^{-1} (0.17 m^{-2} day^{-1}). (For comparison, the flux of relativistic muons on Earth's surface is more than 10^7 m^{-2} day^{-1} [140].) The laboratory space of the first stage (CJPL-1), commissioned in 2010, includes the CDEX (China Dark Matter Experiment) and PandaX (Particle and astrophysical Xenon detector) experiments for the direct registration of DM particles.

The second deepest research laboratory, SNOLAB (Sudbury Neutrino Observatory LABoratory), is located in northern Ontario at a depth of 2070 m (6010 m w.e.) under a flat surface in a former nickel mine [141]. The muon flux is 3×10^{-6} m^{-2} s^{-1} (0.27 m^{-2} day^{-1}). The search for DM particles is carried out in a number of experiments, in particular, DEAP-3600 (Dark matter Experiment using Argon Pulse-shape discrimination 3600), MiniCLEAN (Mini Cryogenic Low-Energy Astrophysics with Noble liquids), PICASSO (Project In CAnada to Search for Supersymmetric Objects), PICO, DAMIC (DArk Matter In CCDs), and SuperCDMS (Super Cryogenic Dark Matter Search) in SNOLAB.

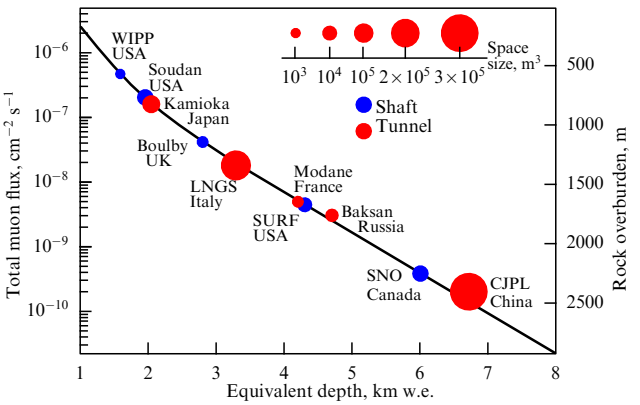

Figure 9. (Color online.) Comparison of the largest underground research laboratories (figure from [139]). The sizes of the dots correspond to the volumes of laboratory space; red or blue color denotes access by road tunnels or shafts, respectively. The ordinate axis shows the measured residual muon fluxes in underground facilities; the black line, the calculation result. WIPP, Waste Isolation Pilot Plant; LNGS, Laboratori Nazionali del Gran Sasso; SURF, Sanford Underground Research Facility; SNO, Sudbury Neutrino Observatory; CJPL, China Jinping Underground Laboratory.

The Modane underground laboratory [142] is located under the Fréjus Mountain in the road tunnel between France and Italy at an average depth of 4800 m w.e., where the muon flux is 5.76×10^{-5} m^{-2} s^{-1} (5 m^{-2} day^{-1}). The laboratory is a platform for experiments in various fields of science requiring a low-radiation background. The main experiments are for the search for DM: EDELWEISS (Expérience pour DÉtecter Les WIMPs En Site Souterrain), EURECA (European Underground Rare Event CAlorimeter), and MIMAC (MIcro-tpc MAtrix of Chambers).

The Gran Sasso Underground Laboratory (Laboratori Nazionali del Gran Sasso, LNGS) of the National Institute for Nuclear Physics (Istituto Nazionale di Fisica Nucleare, INFN) [143] was constructed simultaneously with the road tunnel under the Apennines in central Italy at an average depth of about 1400 m (3650 m w.e.). The rock thickness attenuates the muon flux to 3.7×10^{-2} m^{-2} s^{-1} (26 m^{-2} day^{-1}). The underground facilities consist of three experimental halls, a set of connecting tunnels, and service zones of 18,000 m^2 total area. This laboratory hosted, for example, the OPERA (Oscillation Project with Emulsion-tRacking Apparatus) experiment that discovered oscillations of muon neutrinos into tau neutrinos [37]. At present, the LNGS is carrying out and preparing a series of experiments on the direct search for DM particles (DAMA/LIBRA (DArk MAtter/Large sodium Iodide Bulk for Rare processes), HEIDELBERG–MOSCOW, CRESST (Cryogenic Rare Event Search with Superconducting Thermometers), XENON, NEWSdm (Nuclear Emulsion for WIMPS Search with directional measurement), etc.).

The Boulby Palmer underground laboratory of Sheffield University (Great Britain) [144] is located in a mine at a depth of 1100 m (2850 m w.e.). The total area of the laboratory is about 1500 m^2. The muon flux is 4.1×10^{-4} m^{-2} s^{-1}. The scientific activities of the Boulby laboratory are mainly focused on the search for DM (experiments ZEPLIN-II (ZonEd Proportional scintillation in LIquid Noble gases II) and ZEPLIN-III, LUX (Large Underground Xenon experiment), DRIFT (Directional Recoil Identification From Tracks), and DRIFT-II).

The Japanese underground facility, Kamioka Observatory [145], better known for the experiment with the Super-Kamiokande Neutrino Telescope, also carries out experiments on the direct registration of DM particles (PICO-LON (Planar Inorganic Crystal Observatory for LOw background Neutr(al)inos), XMASS (Xenon MASSive detector), and NEWAGE (NEw generation WIMP search with an Advanced Gaseous tracking device Experiment)). Experiments are performed at a depth of 2700 m w.e. The atmospheric muon flux is attenuated 10^5 times compared to the surface flux [146].

Other, less deep, underground facilities where DM direct registration experiments are conducted include the Soudan underground laboratory, USA [147] (experiments CoGeNT (Coherent Germanium Neutrino Technology), CDMSII, SuperCDMS); the Canfranc underground laboratory, Spain [148] (experiments Anais (Annual modulation with NAI Scintillators), ArDM (Argon Dark Matter)); and the Yangyang underground laboratory, South Korea [149] (experiment COSINE-100 (ConsOrtium between KIMS (Korea Invisible Mass Search) and DM-Ice Sodium IodiNe Experiment 100)).

4.2.2 Scintillation detectors. Scintillators are some of the most popular registration devices in elementary particle physics. When particles pass through a scintillator, atoms or molecules of the medium get excited, which is followed by the emanation of light registered by photodetectors. Experiments on the search for DM mainly use crystals of NaI(Tl) and CsI(Tl) having the best energy resolution (about 8% for an energy of 1 MeV) and the lowest energy threshold among scintillators [150]. Separation of the signal and the background in these detectors is not possible; for this reason, an annual modulation of the signal is used to identify DM interactions. Powders with low contents of uranium, thorium, and potassium are used to decrease the background during crystal growth [151]. For the same purpose, most experiments use active veto systems (see, e.g., [152]).

The DAMA/LIBRA experiment currently being carried out (target mass, 232.8 kg) and its precursor DAMA/NaI (target mass, 87.3 kg) are some of the first experiments on the direct registration of DM particles taking into account annual oscillations of the WIMP signal frequency using a model-independent signature of annual modulation [153]. Measurements are carried out within a 2–6-keV$_{ee}$ energy range (keV$_{ee}$, keV electron equivalent).

The experimental facility is located in the Gran Sasso underground laboratory at a depth of about 1.5 km of mountain rock, which serves as a reliable shield from CR. The experiment uses NaI crystal scintillators with the addition of thallium Tl. Each scintillator is a crystal rod about 10 kg in mass, enclosed into a copper 'brick' for the maximum isolation from background emissions. The crystal is simultaneously a detector and a target, where a WIMP in a collision with the nucleus of a substance induces a flash of light. Induced light is trapped by photomultipliers mounted at the butt ends of the scintillator. The detector is a block of 25 crystals packed into a multilayer casing from materials with minimal intrinsic radioactivity (Fig. 10). The temperature maintained in the facility is constant room temperature, accurate to several thousandths of a degree.

To distinguish signals of WIMP interactions from background events, the following requirements must be met:

— the annual modulation signature should be described by a sine function with a one-year period;

— the modulation amplitude in the region of maximum sensitivity should be within the range of 7 to 30%;

— the annual modulation signature must only be found in a clearly defined low-energy range, where events induced by DM particles can be present;

— a registered detector response is considered to be a signal within only a clearly defined low-energy range, where events induced by DM particles can occur;

— a registered detector response is considered to be a signal if only one of many detectors fires (9 in DAMA/NaI and 25 in DAMA/LIBRA), since the probability of a multiple interaction of DM particles is negligible.

Figure 11 shows the result of observations of annual variations in the DAMA/NaI and DAMA/LIBRA experiments. The plot presents the temporal distribution of the measured signal with subtracted background events over more than 20 years of measurements. The beginning of the DAMA/NaI experiment with a lighter target corresponds to the origin of the abscissa axis; after an interval, the data from the DAMA/LIBRA experiment with a heavier target are shown. The data are fit by a sinusoid and clearly demonstrate the maxima and minima of the detector count with a one-year period.

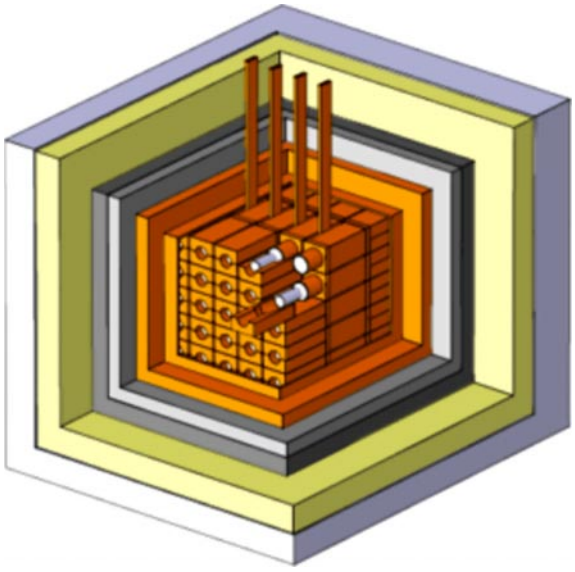

Figure 10. Schematic image of multilayer shield of DAMA/LIBRA detector. (From [154].)

The rigorous selection of signal events, which satisfies the above-described requirements, as well as a multi-level isolation of the background and constant monitoring of the residual radioactivity, enabled reporting with 12.9σ confidence the registered weak annual signal oscillations with an amplitude of about 1–2% [156]. As the DAMA experiment is not capable of separating recoil nuclei and recoil electrons, the obtained data also include cases of WIMP scattering on electrons [157].

However, a number of experiments do not confirm the DAMA results (see, e.g., [158, 159]), supporting the assumption that these data can be interpreted as a contribution from CR muon variations caused by seasonal atmospheric density changes [160].

Experiments using similar technologies are carried out to independently verify the DAMA result in other underground laboratories. The ANAIS experiment [161], like DAMA/LIBRA, is an experiment for the direct detection of annual oscillations of WIMP flashes. The experimental facility is located at the Canfranc underground laboratory. The main aim of the experiment is to independently replicate the DAMA/LIBRA experimental results. The working substance of the ANAIS detector, 112.5 kg in weight, is also NaI(Tl) crystals. The experiment, launched in 2017, is intended to last 5 years as a minimum. One of the major distinctions between the two experiments is the different thicknesses of rock over the facility, 1400 m for Gran Sasso and 850 m for Canfranc, which in the latter case can yield a larger contribution of CR background. The active muon veto system used in ANAIS enables solving this problem.

The ANAIS experimental data for the period from 2017 to 2019 are compared in Fig. 12 with the DAMA/LIBRA results. In this graphical representation, all experimental results are normalized by the function

$$R(t) = R_0 + R_1 \exp\left(-\frac{t}{\tau}\right) + S_{\rm m} \cos\left[\omega(t - t_0)\right], \qquad (5)$$

where R_1 and R_0 are free parameters; τ is a fixed parameter obtained for annual modulations in a corresponding energy range; and parameter $S_{\rm m}$ equals zero for the null hypothesis (the absence of annual modulations at a confidence level of 1σ) and has different values at different model approaches.

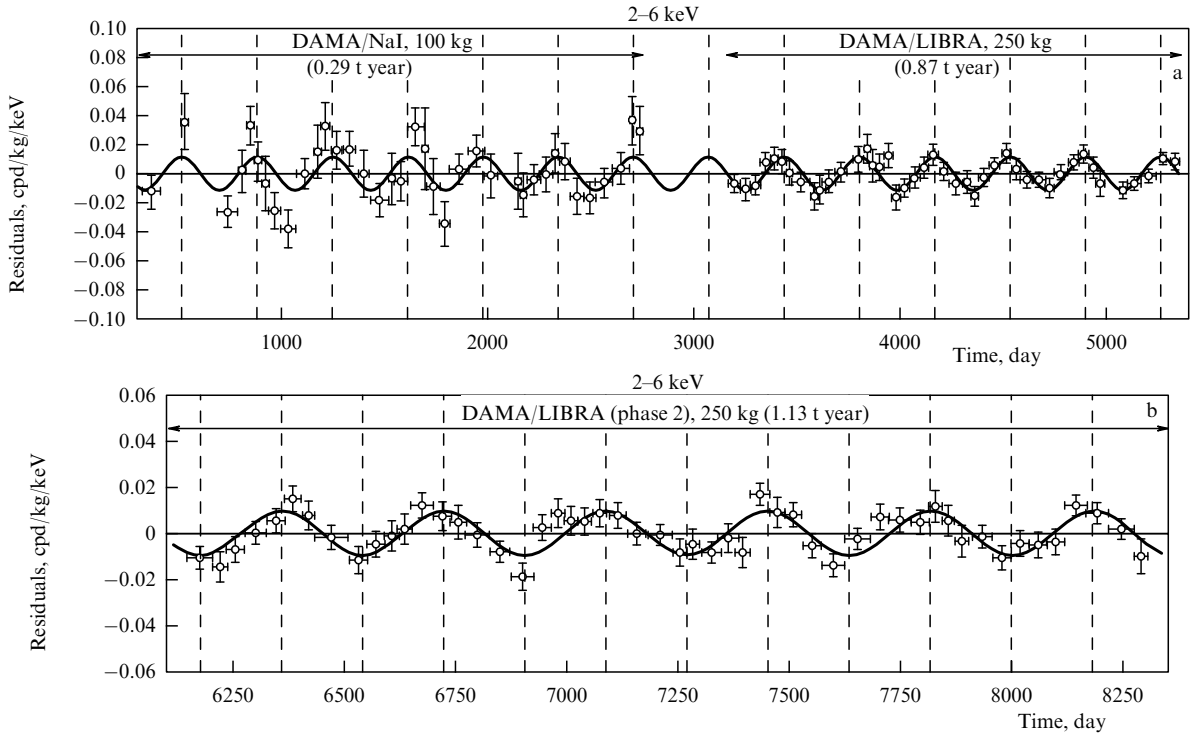

Figure 11. Detector firing rate as a function of time within the energy region of 2–6 keV over entire period of measurements (interval of measurements in Fig. (b) continues interval in Fig. (a)). Only alternating part of signal remaining after subtraction of the constant background is shown. Solid line represents a cosine function describing one-year period modulations. Maxima and minima on 2 June and 2 December are shown by dashed lines, respectively. Figure (a), from [155]; Fig. (b), from [156].

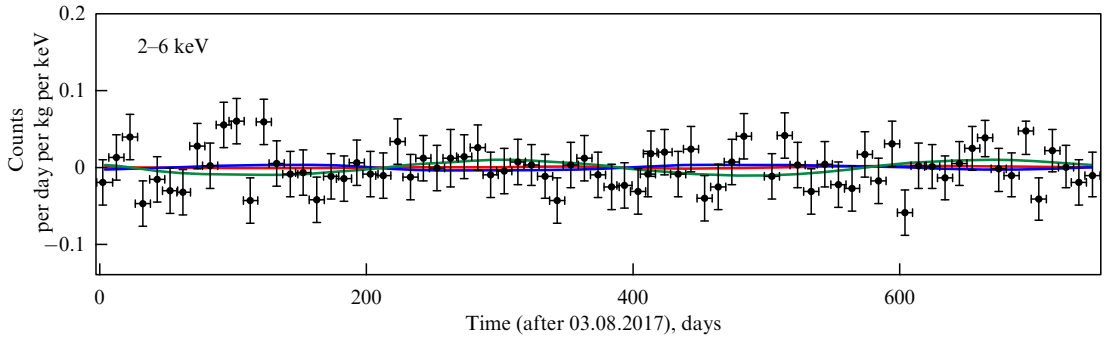

Figure 12. (Color online.) Detector firing rate as a function of time within energy region of 2–6 keV in the ANAIS experiment (data from 2017–2019 are shown by dots with error bars). Similar DAMA/LIBRA data are shown (green curve) for comparison. Blue and red curves represent approximations of ANAIS experimental data for, respectively, the model-independent hypothesis and the null hypothesis, describing annual modulations. (From [161].)

The ANAIS results are seen to agree well with the null hypothesis. Discrepancies in the experimental data of the ANAIS and DAMA/LIBRA experiments are explained by different sensitivities of signal registration.

Yet another experiment for the direct detection of WIMP is the COSINE-100 experiment [162] conducted in the Yangyang underground laboratory (South Korea) at a depth of 700 m. The experiment searches for DM interactions in NaI(Tl) scintillating crystals; simultaneously, CR muons are registered to assess the effect of their annual modulation on the produced result [163]. The COSINE-100 detector structure slightly differs from that of DAMA/LIBRA and ANAIS. An array of eight NaI(Tl) crystals is immersed in the liquid scintillator, which enables the separation of the background, developed by radiogenic particles from NaI(Tl) crystal components, owing to the implementation of the requirement for signal anticoincidence in crystals and in liquid scintillators, which is of crucial significance in the analysis of annual modulations. Moreover, the high thermal capacity of the liquid scintillator maintains a stable temperature of the liquid and NaI(Tl) crystals at the level of $24.20 \pm 0.05\,^{\circ}\mathrm{C}$.

Analysis of the data for the first stage of COSINE-100 operation found no features of signal excess over the expected background. From the viewpoint of the standard DM halo model, this result rules out WIMP–nucleon spin-independent interactions as the cause of annual modulation observed by the DAMA collaboration with a 90% confidence [164].

4.2.3 Liquefied inert gas detectors. The liquid-phase noble gases xenon and argon readily ionized with the passage of charged particles are an efficient basis of homogeneous and compact large-mass scintillation detectors. Of all the noble gases, only xenon and argon are widely used at present in DM detectors, though neon proposed for registration of low-energy neutrinos can also be used in the search for DM particles [165].

Xenon and argon are chemically inert and can be subjected to deep purification from various gaseous impurities. The concentration of xenon in the atmosphere is relatively small, which makes it more expensive than natural argon. On the other hand, xenon contains no radioactive isotopes except ^{136}Xe, which is a source of double-beta decay with the half-life of $(2.165 \pm 0.016 \pm 0.059) \times 10^{21}$ years [166]. The cross section of WIMP scattering on xenon nuclei is relatively high owing to its large atomic mass. In addition, due to the high density and large charge of the nucleus, gamma rays have very short interaction lengths (self-shielding). Liquid xenon (LXe) brightly scintillates at a wavelength of 178 nm, remaining transparent, which enables effective examination of large volumes by arrays of photomultiplier tubes (PMTs) registering flashes of light during the passage of a particle. In this regard, the total amount of registered light is proportional to the energy released.

Liquid argon (LAr) is a 'lighter' version of LXe. In contrast to LXe, in LAr the temporal structure of a scintillator pulse depends on the nature of the event, which makes it possible to effectively separate the signal from the background by scintillator pulse shape discrimination (PSD). However, the reliable use of PSD requires a relatively large energy threshold, which limits the sensitivity of argon to small-mass WIMPs.

Argon scintillates at a wavelength of 128 nm. Due to the impossibility of effective direct registration of hard UV-range photons, detectors use a special material, a wavelength shifter (WLS), whose molecules absorb UV photons and emit visible-range photons efficiently registered by standard PMTs. The most widespread WLS is tetraphenyl butadiene (TPB), distinguished by a rapid radiative recombination of electron–hole pairs in oligomer benzene rings. A rapid response is required to register nondistorted waveforms of the fast scintillation component; it decays with a time constant of the order of several nanoseconds, which is essential for PSD analysis. TPB registers especially well hard UV photons owing to a large Stokes shift. The fluorescence decay time is about 1.68 ns, and the recombination process is not substantially slowed down at cryogenic temperatures. TPB coatings are sufficiently durable, are easy to apply, and are resistant to mechanical abrasion.

A significant drawback of argon is its activation by cosmic rays, which leads to the formation of the radioactive isotope ^{39}Ar via the reaction $^{40}\mathrm{Ar}(\mathrm{n}, 2\mathrm{n})^{39}\mathrm{Ar}$ with an energy threshold of about 1 MeV. The measured concentration ratio of ^{39}Ar and ^{40}Ar is 8.1×10^{-16}, as a result of which the specific activity of ^{39}Ar is 1 Bq kg^{-1} [167].

Energy losses of a charged particle are redistributed between the ionization and excitation of atoms of the medium. Both processes lead to the emission of scintillation photons via the following processes [168]:

1)

$$\mathrm{R}^{*} + 2\mathrm{R} \to \mathrm{R}_2^{*} + \mathrm{R}\,, \tag{6}$$

$$\mathrm{R}_2^{*} \to 2\mathrm{R} + \gamma\,; \tag{7}$$

2)

$$\mathrm{R}^{+} + \mathrm{R} \to \mathrm{R}_2^{+}\,, \tag{8}$$

$$R^{**} \to R^{*} + \text{heat}\,, \tag{9}$$

$$R_2^{*} \to 2R + \gamma\,, \tag{10}$$

$$R_2^{+} + e^{-} \to R^{**} + R\,, \tag{11}$$

$$R^{*} + 2R \to R_2^{*} + R\,, \tag{12}$$

where R^{*} and R^{+} are excited and ionized atoms of the medium, respectively; γ is the emitted photon; and $R^{**} \to R^{*} + \text{heat}$ is the nonradiative transition between the levels. In both processes, dimer R_2^{*} relaxes from the lower excited state to the main state to emit one UV photon. The large distance between these levels makes impossible other channels, such as nonradiative transition. Scintillation emission in LAr and LXe has two temporal components determined by transitions from the singlet and triplet states of dimer R_2^{*}. The shorter decay form emerges in the transition from the singlet state; the longer, from the triplet state. This difference is the basis of the PSD analysis, especially efficient for liquid argon, where the separation in time is of the order of 1.5 μs [169–171].

PSD analysis is indispensable in liquid argon, where it enables successful control of the radioactive background from ^{39}Ar. To reduce the concentration of ^{39}Ar, it was suggested to use argon extracted from underground sources (Underground Ar, UAr) with subsequent additional purification (Depleted Ar, DAr) [172].

Experimenters have to control numerous sources of background events capable of simulating genuine WIMP scattering. To minimize gamma quantum and neutron fluxes generated inside detector components, materials with a minimal radiation background are chosen. To prevent the contamination of surfaces with radon and products of its decay, all sensitive detector components are assembled in pure chambers, and cryogenic systems are equipped with special filters constantly removing radon and its decay products during the recirculation of argon and xenon. The exact measurement of the coordinates inside the detector makes it possible to sample only those events occurring in the internal (active) volume, away from the detector's walls and nodes, where, owing to the shielding effect, gamma radiation barely penetrates, and neutrons can be identified due to multiple scattering in the inner volume. Finally, to rule out background events caused by external particles, many experiments use active muon and neutron veto systems.

Detectors based on liquid noble gases are usually of two classes: single-phase and double-phase. *Single-phase detectors,* as follows from the name, contain only one liquid phase of the active substance (experiments MiniCLEAN [173], DEAP-3600 [174], and XMASS [175]). Single-phase detectors are conceptually simple and represent a spherical bulk of noble liquid scanned by the enclosing array of low-radioactive PMTs. The spherical form enables minimal contact of the liquid target with the cryostat material, which is usually an acrylic that can be fabricated by a controlled radiopure technique. This material is an efficient neutron absorber and possesses useful optical, mechanical, and thermal properties. The ability to withstand large temperature gradients makes it possible to use acrylic to produce light guides passing the signal from the cryogenic inner surface to the outer surface connected to the PMT, at close-to-room temperature.

The XMASS experiment based on a single-phase scintillation detector is located at the Kamioka underground laboratory. It consists of a water Cherenkov outer veto detector and a spherical inner detector with 832 kg of liquid xenon enclosed with low-radioactive PMTs 6.5 cm in diameter. To eliminate background events, the XMASS uses an outer layer of 735-kg LXe as well as an active veto. At the end of 2018, the collaboration reported that, after 705.9 days of operation with an active volume of 97 kg, they achieved a scattering cross section lower limit of 2.2×10^{-44} cm^2 for WIMPs of 60 GeV/c^2 mass [175].

The DEAP-3600 experiment located at a depth of 2 km in the SNOLAB underground laboratory contains a cryostat consisting of a spherical acrylic vessel with a wall thickness of 5 cm, which can hold up to 3600 kg LAr (at present, the detector operates with 3279 kg LAr). The inner surface of the cryostat is coated with a TPB layer 3 μm thick. The active volume is scanned by means of 255 high quantum-efficient eight-inch PMTs fabricated from low-radioactive glass. The outer steel shell is immersed in a shield tank with ultrapure water and is equipped with 48 PMTs that serve as a muon veto. The readout electronics are optimized for the PSD analysis. In 2019, using the results of 231 days of operation, the DEAP collaboration obtained an estimate for the scattering cross section lower limit of 3.9×10^{-45} cm^2 (1.5×10^{-44} cm^2) for WIMPs of 100 GeV/c^2 mass (1 TeV/c^2) with a 90% confidence [174]. To date, this is the record result for a spin-independent WIMP scattering cross section for detectors based on liquid argon.

The same laboratory conducts the MiniCLEAN experiment [176] intended for the use of over 500 kg of a liquid cryogen, either LAr or neon (LNe). This experiment is a demo version of a future detector 50 to 100 tons in weight. Similar to DEAP and XMASS, it uses a modular design of spherical geometry and relies on the PSD analyses and an active muon veto to rule out background events. To analyze the efficiency of the PSD analysis, MiniCLEAN uses liquid argon enriched with ^{39}Ar with an activity level exceeding the level of natural argon by approximately tenfold. These measurements are assumed to improve the PSD efficiency estimate by more than two orders of magnitude.

A unique feature of single-phase detectors is the possibility of checking the DM particle detection hypothesis by replacing the active substance. Thus, if WIMP candidates are found in an LAr-based detector, then it is necessary to repeat the exposure using argon enriched with ^{39}Ar with an activity exceeding by tenfold that of natural argon. If in this case the event registration rate also increases tenfold, this would mean that in the former experiment the detector registered a signal from the decay of ^{39}Ar, not a WIMP. If, however, the registration rate remains invariable, the experiment should be repeated one more time, replacing in this case LAr by LNe. This replacement of the detector's active material would decrease the estimate for the WIMP scattering cross section almost ten times, which, as is expected, would lead to a proportional decrease in the signal registration rate in the detector. If this does not occur, it would mean that the detector registers an unaccounted-for neutron background, not WIMP interactions. This two-stage check would make it possible to unambiguously rule out the effects of the two most dangerous false-positive signals and is an indisputable advantage of single-phase detectors based on liquefied noble gases [177]. The possibility of changing the detector's active substance to check the signal is a potent and unique feature of single-phase detectors.

Double-phase detectors based on liquid noble gases are one of the central classes of detector technologies used in the direct search for DM. Usually, these detectors are constructed

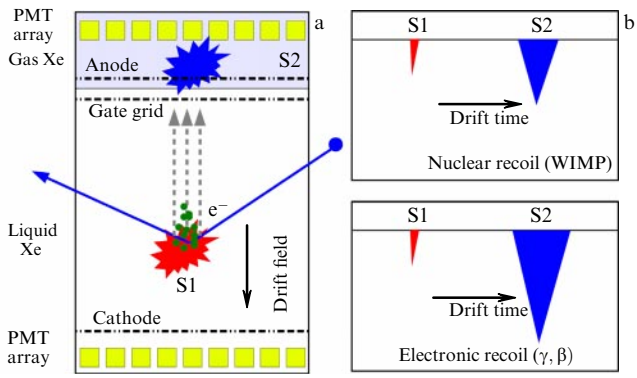

Figure 13. (a) Operating principle of the XENON double-phase liquid-gas time-projection chamber (TPC). (b) Diagrams of signals from two types of events. Different brightness ratios of the secondary (electroluminescent, S2) and primary (fluorescent, S1) signals enable discriminating between recoil nuclei from WIMPs and neutrons and recoil electrons from gamma and beta backgrounds. (From [178].)

as a time projection chamber (TPC) with the liquid and gas phases. As is shown in Fig. 13a, a fast signal of scintillation light (S1) is generated in the active volume with the interaction of a particle; the signal is collected mainly by PMTs arranged in the lower part of the detector. Ionization electrons created at the time of the primary interaction drift in a homogeneous electric field towards the gas field are extracted into it and create an electroluminescent pulse (S2). The x, y interaction coordinates can be determined by the spatial distribution of signal S2 registered by the upper PMT array. The third coordinate, z, is determined by assessing the time difference between signals S1 and S2 taking into account the average velocity of electron drift in the field. This technique makes it possible to reconstruct the 3D position of events and tracks. Furthermore, the temporal structure of signal S1 and the primary-to-secondary signal ratio enables separating recoil nuclei and recoil electrons with an efficiency determined by the noble gas, applied electric field intensity, and active substance purity.

TPC double-phase detectors based on LXe are used in the XENON1T [179], PandaX-II [180], LUX [181], and ZEPLIN-III [182] experiments. LXe-based TPCs provide viable constraints on the spin-dependent WIMP scattering cross section, using isotopes ^{129}Xe and ^{131}Xe. Results published by the XENON100 [183], LUX [181], and PandaX-II [182] experiments are shown in Fig. 14. It should be noted that spin-dependent interactions cannot be investigated in LAr detectors due to the absence of isotopes with nonzero nuclear spin.

The strictest constraints on the WIMP–nucleon spin-independent cross section were obtained by means of double-phase TPCs using liquid xenon as an active target material. Recently, the XENON1T experiment published data on the WIMP scattering cross section (7.7×10^{-47} cm^2 for a mass of 35 GeV/c^2 [185]), which improved the result of the LUX [181] and PandaX-II [180] experiments (Fig. 15). Owing to the scalability of double-phase detector technology, future multi-ton LXe experiments, such as LUX-ZEPLIN [186], XENONnT, and DARWIN (DARk matter WImp search with liquid xenoN) [187] are expected to improve the sensitivity to WIMPs by about three orders of magnitude and to approach closely the so-called 'neutrino limit' [188].

Liquid argon is also widely used in double-phase experiments, such as DarkSide [190]. The DarkSide-50 collaboration used argon from underground sources; it contains 1000 times less cosmogenically activated ^{39}Ar than natural argon. Four leading DM search experiments using liquid argon technologies (ArDM at the Canfranc laboratory, DarkSide-50 at LNGS, DEAP-3600, and MiniCLEAN at SNOLAB) agreed to unite efforts to implement an integrated direct DM detection program within the framework of the DarkSide-20k experiment [191]. This experiment plans to achieve a WIMP direct detection sensitivity reaching 1.2×10^{-47} cm^2 at a mass of 1 TeV/c^2. DarkSide-20k would be able to achieve this goal using a double-phase TPC of a total mass of 23 tons (active mass, 20 tons). It is assumed that argon extracted from underground sources and additionally purified would be used. Instead of traditional PMTs, silicon photomultipliers (SiPMs) would be used, because they have a higher photon detection efficiency and a much better single photon resolution; all that at a considerably lower bias voltage. SiPMs can also be efficiently integrated into panels, which cover large areas and have a better radiopurity than PMTs.

It is expected that DarkSide-20k would be able to operate up to ten years, accumulating up to 200 t year of exposures and achieving a sensitivity of 7.4×10^{-48} cm^2. The success of the DarkSide-20k experiment can be a landmark on the way to the further development of LAr-based double-phase TPC technology for the search for DM signals (see [189]).

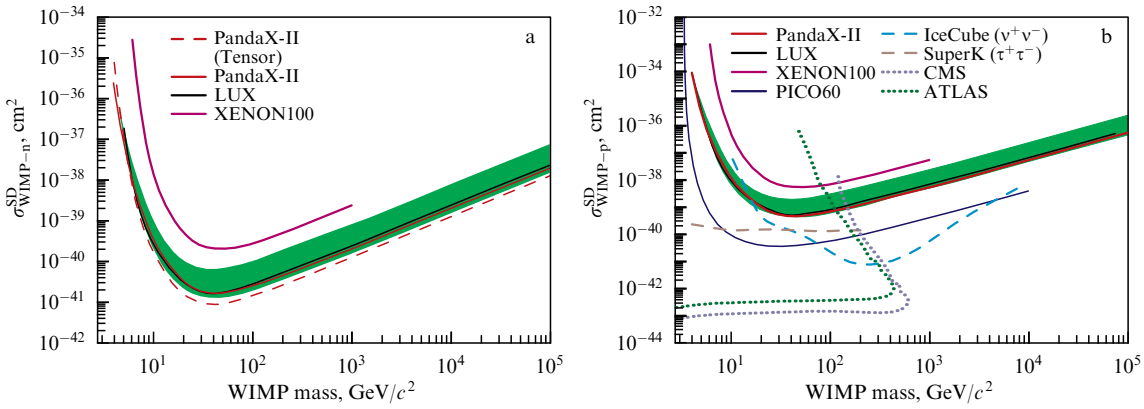

Figure 14. (Color online.) Upper limits for WIMP–neutron (a) and WIMP–proton (b) spin-dependent scattering cross sections for PandaX-II, LUX, and XENON100 experiments [184].

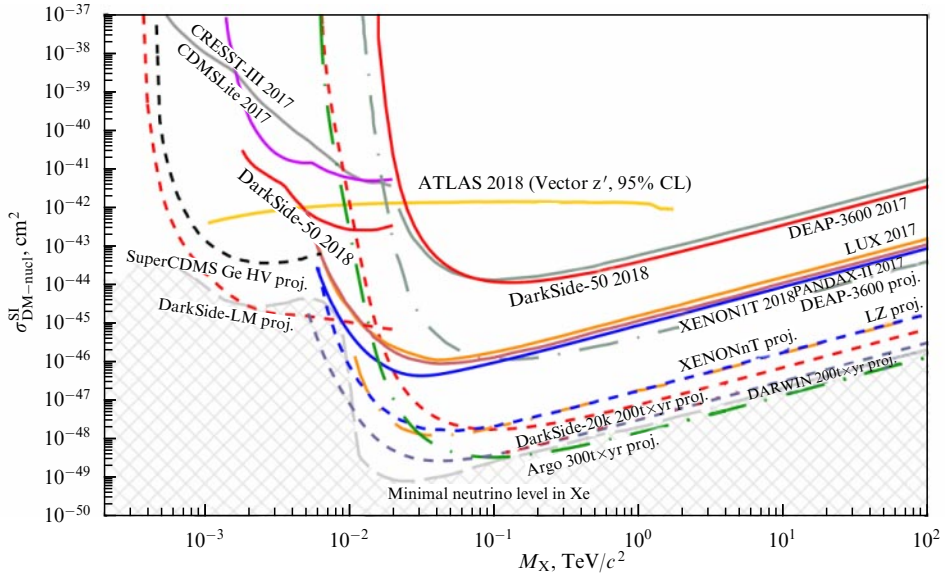

Figure 15. (Color online.) 90% confidence level exclusion curves showing the results of leading experiments on direct DM searches (continuous lines) and accelerating DM searches (region above yellow line) compared with sensitivities of future direct search experiments based on germanium, xenon, and argon (dashed lines). 95% confidence level limit from ATLAS (A Toroidal Large hadron collider ApparatuS) experiment is shown for a model in which WIMPs interact with ordinary matter as a Dirac fermion via a vector mediator with coupling strengths to quarks, leptons, and WIMPs of 0.25, 0.01, and 1, respectively. (From [189].)

4.2.4 Semiconductor detectors. In interactions with WIMPs, recoil nuclei can be found in the form of ionization pulses. *Germanium detectors* operated in the ionization mode have a very low energy threshold enabling the search for WIMPs up to masses of several GeV [192]. The major advantage of these detectors is their resolving power. The high energy resolution of detectors (about 0.15% for 1.3 MeV) makes it possible to identify background sources from radioactive impurities. To decrease the level of noise, detectors are cooled to the liquid nitrogen temperature of ~ 77 K [193].

The technology of low-background germanium detectors first applied in 1987 [194] has been actively improved and is used at present. Thus, the CoGeNT experiment using p-type point contact germanium detectors achieved an energy threshold of 500 eV_{ee} [195].

The CoGeNT detector located at the Soudan underground laboratory counted events for 3.4 years taking into account annual modulation. Count rate modulation within the energy interval of 0.5–2 keV_{ee} was found with a signal confidence of 2.2σ; the amplitude of the signal proved to be 4–7 times greater than the expected value. The signal was interpreted to be the result of WIMP interactions (mass of 8 GeV/c^2; cross section of about 2.5×10^{-41} cm^2). However, an independent analysis of the CoGeNT experiment data showed no occurrence of a signal [196].

The experiment also assessed the sensitivity of the CoGeNT detector for the search for signals from axions. These particles could have interacted in a germanium detector via the axioelectric effect (similar to the photoelectric effect) to form a recoil electron with an energy corresponding to the axion mass [197]. The absence of a corresponding peak in the experimental spectrum enabled assessing the limits of the axion–electron coupling [198].

To avoid crystals of large sizes with a relatively high noise, the China dark matter experiment (CDEX) [199] makes use of an assembly of p-type point contact germanium detectors (5 g each) enclosed in an NaI(Tl) crystal scintillator that serves as an anti-coincidence detector. The low background required for the search for WIMPs in the low-boundary region of masses (< 10 GeV/c^2) is provided for, among other things, by the depth of the CJPL laboratory (see Section 4.2.1).

Each crystalline cylinder of the detector has an n^+-type contact on the outer surface and a p^+-type point contact as the central electrode. Electron–hole pairs are formed upon the interaction of particles with Ge atoms. Under the action of an electric field, electrons and holes drift to the opposite electrodes, and signals are induced at the p^+- and n^+-electrodes. Owing to the structure of the electrode, holes near the surface drift considerably more slowly; for this reason, the signal pulse has a long rise time and a relatively small amplitude. Such a detector possesses the ability to discriminate between surface (background) and bulk (signal) events. This technology enables reducing the energy threshold of the facility to several hundred electron volts.

In 2014, the collaboration deployed a CDEX-1 detector with an energy threshold of 160 eV_{ee}. Using the results of 4.2 years of CDEX-1 operation, the annual modulation of the detected event rate was analyzed, excluding the conclusions of DAMA/LIBRA and CoGeNT with a confidence of 99.99% and 98.0%, respectively [200].

Widespread interest in the issue of DM particle registration by semiconductor detectors has lately been due to a subdominant atomic effect, the so-called Migdal effect [201]. Atomic electrons around the nucleus of the target are usually assumed to immediately follow the motion of the recoil nucleus. In reality, however, electrons need some time to catch up, which leads to the ionization and excitation of atoms. In other words, the bias between the interacting nucleus and enclosing electrons can lead to an additional excitation energy higher than the detector's threshold, which expands the range of masses of registered DM particles towards its decrease. Accounting for this effect in the CDEX experiment enabled reducing the detector's registration

threshold by more than an order of magnitude (to approximately 50 MeV/c^2) [202].

In 2017, an upgraded experiment CDEX-10 was put into operation, with a total detector mass of about 10 kg. The first obtained data enabled assessing the WIMP–nucleon interaction cross section boundary as 8×10^{-42} cm^2 for a WIMP mass of 5 GeV/c^2 [203]. Moreover, the CDEX data are used for the search for rare processes involving axions [204], bosonic DM [205], and dark photons [206]. A long-term goal of the collaboration is the CDEX-1T experiment with a detector 1 ton in weight.

The DAMIC experiment [207] is being carried out at present at the SNOLAB underground laboratory. The experiment uses silicon CCD semiconductor detectors for the search for DM particles. The unique sensitivity and low noise of the CCD matrices used provide an unprecedented low energy threshold of the detector, several ten eV, which enables the investigation of signals from interactions of DM particles with low masses (less than 10 GeV/c^2). The experiment searches for SuperWIMPs and 'hidden sector' particles. Similar to common photons, 'hidden' photons can be absorbed by electrons in the bulk of the silicon detector and lead to an ionization signal. The DAMIC experiment considers ionization signals within the range of (1–11) e^-, which can have a bearing on the absorption of 'hidden' photons with masses of 1.2–30 eV/c^2.

The experiment established the limits of the direct detection of DM scattering on electrons within the range of masses from 0.6 MeV/c^2 to 6 MeV/c^2, as well as constraints on the direct detection of 'hidden' photons within the range of masses from 3 to 12 eV/c^2 [208]. Further studies are planned to be carried out in the Modane underground laboratory using the larger mass detector, DAMIC-M.

4.2.5 Cryogenic phonon bolometers. Despite the high sensitivity of semiconductor detectors, these experiments on the direct registration of DM could not find convincing evidence of its existence. This could have been interpreted as a failure of the WIMP hypothesis; however, an alternative explanation is that WIMPs can be lighter than assumed and that the energy released by recoil nuclei in the detector is lower than the experimental thresholds achieved [209]. As a result, interest arose in experiments with lower thresholds for recoil nuclei, in particular, in cryogenic bolometers, which can separate recoil nuclei and recoil electrons, significantly reducing the background.

Cryogenic bolometers are combined devices, independently registering the ionization (scintillation) and thermal signals from one source (see, e.g., [210]). Their operating principle consists in the fact that thermosensitive element of the bolometer heats up upon the absorbing some kinds of emission (photons, phonons), as a result of which its resistance changes. To increase the accuracy of measurements, the device is cooled to the temperature of liquid helium.

In the experiment, the nucleus recoil energy is assessed taking into account the quenching effect, i.e., the loss of signal due to various mechanisms. In the detector, only part of recoil energy QE is released; its value depends on the type of detector and target. The quenching factor Q, determined as the ratio between the ionization caused by the energy of the recoil nucleus (expressed in keV$_r$) and the ionization due to the recoil of the same energy by the electron (expressed in keV$_{ee}$), is for various detectors from 0.1 to 0.6. For instance, for germanium detectors, the quenching factor is approximately 0.25. With the registration of a signal by scintillation or ionization detectors in cryogenic bolometers, the energy dependence of signal quenching enables discriminating between the recoil nucleus and recoil electron.

In cryogenic phonon bolometers, some of the energy passed by the DM particle in the target crystal is transformed into phonons, which can be separated into thermal and athermal. Thermal phonons are related to the thermal equilibrium of the medium, and their energies are determined by the induced temperature increase of the medium. Part of the energy is passed to phonons having larger free path lengths (athermal phonons), which carry information not only about the value of energy release but also about the point of interaction. In a crystal placed in an electric field, drifting electron–hole pairs pass additional energy to the crystal lattice, thus enhancing the phonon signal (Neganov–Trofimov–Luke (NTL) effect [211]), which should be taken into account when assessing the recoil energy; this enables decreasing the detector's energy threshold. Irrespective of the readout technology, the phonon signal is directly proportional to the energy release and can be used to determine the recoil energy.

In a series of Cryogenic Dark Matter Search (CDMS) experiments (CDMS [212], CDMSII [213], SuperCDMS in SOUDAN [214], SuperCDMS in SNOLAB [215]), DM particles are searched for using germanium and silicon bolometers at the Soudan and SNOLAB underground laboratories.

These experiments determine two energy parameters for each registered event: the ionization energy, proportional to the number of collected electron–hole pairs, and the recoil energy, determined by subtraction of the contribution from NTL phonons from the total measured phonon energy. The ratio of ionization energy to recoil energy, the so-called ionization yield, is for recoil nuclei in germanium approximately one third that for recoil electrons. The ionization yield is a key parameter making it possible to discriminate between recoil nuclei (e.g., from interactions with DM) and background recoil electrons. The background is mainly formed by signals on the surface of semiconductor detectors, where the ionization yield is decreased, and recoil electrons can be mistaken for recoil nuclei.

The search for signals from WIMPs is performed within the limits of the fiducial phase volume for energy release in the outer ionization sensor [216]. The measurement of phonon thermal-pulse arrival times and a comparison of signal amplitudes in several sensors enable determining the fiducial volume and decreasing the background level. The use of this procedure, fiducialization, results in a very low probability of interpreting surface events from recoil electrons as bulk events from recoil nuclei: $< 1.7 \times 10^{-5}$ for energies of 8–115 keV. As a result, the sensitivity of SuperCDMS instruments enables WIMP searches up to masses of ~ 0.5 GeV/c^2.

Analysis of the data from the CDMS II experiment enabled detecting three signals in the silicon detector, which were interpreted as signals from WIMPs with masses of the order of 10 GeV/c^2. The probability that this is anomalous background noise is only 0.19%, which indicates a signal probability of 99.8% (3σ) [217]. In 2014, the results of the SOUDAN SuperCDMS experiment were published, which contained 11 signals from WIMPs with masses of less than 30 GeV/c^2 [218] and made it possible to find the upper limit of the WIMP–nucleon spin-independent cross section of 1.2×10^{-42} cm^2 at 8 GeV/c^2. The second stage of the

SuperCDMS experiment in the deeper SNOLAB laboratory was planned to be launched in 2020.

A similar concept of the detector is used in the EDELWEISS experiments with a stepwise increase of germanium detector mass; the experiments are carried out in the Modane underground laboratory. The signal is measured by thermal phonons. As thermal phonons carry no information about the interaction point in the space of the crystal, and surface background events dominate within the range of the WIMP search, use is made of an alternate structure of charge readout, which makes it possible to identify surface events by comparing the shape of thermal signals on different sides of the detector [219].

In the EDELWEISS-II experiment, the method of identifying surface events with a reduced ionization yield made it possible to obtain a background event rejection coefficient of more than 10^4. At the last stage of the experiment (EDELWEISS-III [220]), the detectors were equipped with sets of digitized electrodes, which made it possible to refine the selection of interactions by discarding events on the detector's surface. As a result, an increase in the fiducial volume up to 625 g per detector enabled reducing the region of WIMP search to a mass of 4 GeV$/c^2$ and establishing the upper limit for the spin-independent WIMP–nucleon scattering cross section for particles with masses of 5 GeV$/c^2$ equal to 4.3×10^{-40} cm^2 [221]. It is planned that the next upgrade of the EDELWEISS experiment will enable searches for DM particles in the region below 800 eV$/c^2$.

The CRESST experiments, aimed at studying the elastic coherent scattering of DM particles on target nuclei, make use of scintillation light in crystals of Al_2O_3 (CRESST) or $CaWO_4$ (CRESST-II and CRESST-III), besides the phonon signal [222, 223]. One detector module consists of a crystal target simultaneously performing the role of a cryogenic calorimeter ('phonon channel') and an adjacent detector for registration of scintillation photons ('light channel'). The phonon channel is intended to measure the energy passed to the crystal nucleus upon WIMP–nucleus elastic scattering, and the light signal makes it possible to discriminate the recoil nucleus and recoil electron, because the nucleus and electron of the same energy significantly differ by the yield of scintillation light. Recoil nuclei produce less light; therefore, more energy is released in the phonon detector. An efficient suppression of the background from electrons is achieved by the simultaneous measurement of the phonon and light signals.

The phonon and light signals are read out by two tungsten detectors at the edge of the superconducting transition (transition-edge sensors, TESs). The surfaces of the crystals are treated so as to avoid absorption of photons or total internal reflection. Taking into account the low energy threshold of the detectors (lower than 100 eV) and the use of light nuclei as targets, the experiment is aimed at registering low-mass WIMP particles (lower than ≈ 2 GeV$/c^2$).

The treatment of the data from the second phase of the experiment (CRESSTII) [224] yielded four events statistically incompatible with the background. These events may be indicative of an additional source of recoil nuclei in the crystal, besides the background, which could be interpreted as an interaction with a WIMP 11.6 GeV$/c^2$ in mass with an interaction cross section of 3.7×10^{-41} cm^2 (4.2σ) or a mass of 25.3 GeV$/c^2$ with a cross section of 1.6×10^{-42} cm^2 (4.7σ). As a result, it was concluded that the experiment indicated the existence of light WIMPs, which, however, found no confirmation in other experiments (XENON100, CDMS II).

The advanced technology of filtration in the CRESST-III experiment extended the sensitivity range with respect to the mass up to 160 MeV$/c^2$ [225]. However, in the new version of the experiment, the event rate is observed to rise, which is incompatible with the assumption of a flat background and is indicative of a decreased sensitivity of the detector to WIMP–nucleus interactions. Owing to this, the main task of the experiment at this stage is to analyze the nature of the low-energy background.

4.2.6 Bubble chambers. In the context of the search for DM, experimental physics is seeing the return of the superheated liquids technology implemented in the form of bubble chambers and droplet detectors [226]. The advantage of this technology is that, being close to the phase transition temperature, bubble chambers are insensitive to the minimum ionizing background, which usually dominates over the background in other DM detectors, i.e., the background from gamma radiation, X-ray radiation, and electrons from decaying isotopes is blocked. The remaining radiation capable of inducing a signal are alpha-particles and recoil nuclei from interactions with neutrons.

The experiments use refrigerant targets operating in a superheated state slightly lower than the boiling temperature. Recoil nuclei are registered by means of the bubble-initiated process they induce; to form these bubbles, a phase transition of the medium is required. The detector is a threshold device, in which some minimal energy release is required to induce a phase transition. The transition from a droplet of liquid to a bubble of vapor is of an explosive character and is accompanied by an acoustic-range signal, which is fixed by piezoelectric sensors and enables separating signals from α-particles that have a higher acoustic emission compared with signals from recoil nuclei. Upon completion of the cycle, the medium is restored by compressing the liquid, followed by decompression to a value lower than the vapor pressure.

The energy threshold of these detectors can be controlled by changing the temperature and/or pressure. As a result, the detectors may reach an energy threshold of the registration of recoil nuclei of the order of several keV [227]. The mass of a target does not usually exceed several kilograms, and the considered detectors present no competition to larger detectors in the spin-independent sector of interactions. However, the content of fluorine with an unpaired number of protons in the atom in the active liquid (e.g., C_2ClF_5, C_3ClF_8, C_3F_8, C_4F_{10}) makes these detectors sensitive to spin-dependent interactions [228]. Note that detectors based on germanium or liquid xenon have unpaired neutrons and, therefore, a lower sensitivity to proton coupling. That is, bubble chambers have an advantage namely in the spin-dependent sector.

To retain bubbles, droplet detectors use a water-based polymer with a crosslinking agent; this leads to a reduction in the detector's dead time, because small droplets can pass through the phase transition simultaneously. Such a detector can stay active for a much longer time than the classical bubble chamber.

Droplet detectors were used in the PICASSO experiment to search for neutralinos [229]. The project registered a signal at the phase transition of superheated liquid droplets of fluorine-containing refrigerants dispersed in a polymerized gel matrix. As in bubble chambers, an acoustic signal was used to mitigate the α-particle background.

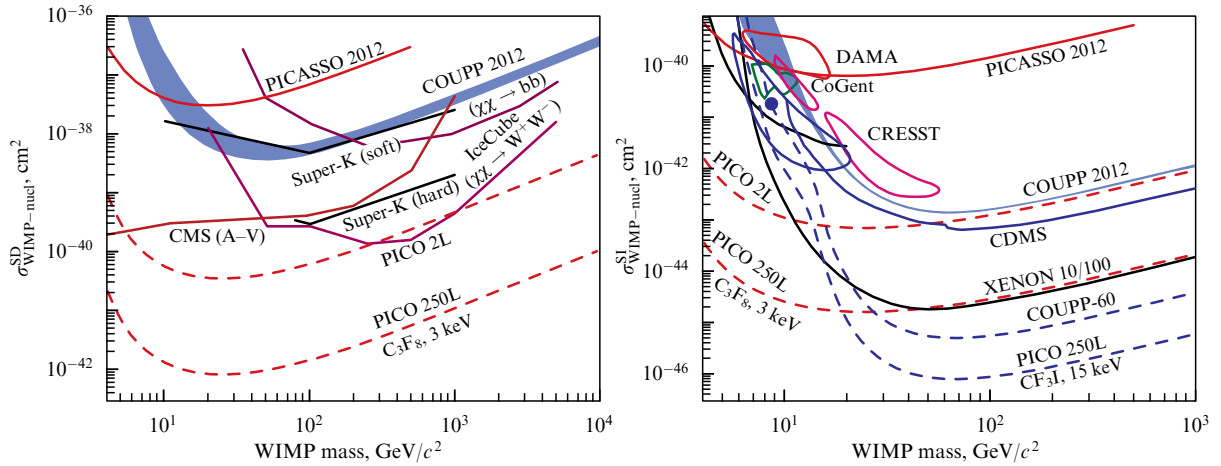

Figure 16. (Color online.) Range of research by PICASSO, COUPP, and PICO experiments using C_3F_8 (red lines) and CF_3I (blue lines) as compared with other experiments. (From [234].)

The recoil energy threshold achieved in the PICASSO experiment was 1.7 keV, which provided for its sensitivity to interactions of WIMPs with masses lower than 10 GeV/c^2; however, no DM signal was found. The cross section limit for WIMP scattering on protons was determined as 3.2×10^{-38} cm^2 in the spin-dependent sector for WIMPs with masses of 20 GeV/c^2 with 90% confidence. In the spin-independent sector for masses of the order of 7 GeV/c^2 (the region of the CoGeNT and DAMA/LIBRA experiments), cross sections greater than 1.41×10^{-40} cm^2 were excluded [230].

The COUPP experiment (Chicagoland Observatory for Underground Particle Physics), with bubble chambers from 2 up to 40 liters in volume, carried out in the MINOS (Main Injector Neutrino Oscillation Search) (Fermi National Accelerator Laboratory) and SNOLAB underground laboratories, achieved a 99.3% efficiency of α-particle signal rejection [231]. As an active liquid, CF_3I was used, which enabled the detector's sensitivity in both the spin-dependent and spin-independent sectors due to fluorine and iodine contents in the target. The transparency of the bubble chamber's working medium enabled determining the coordinates of each bubble to an accuracy of several millimeters by photographing the event with CCD cameras at a speed of 100 frames per second (which is impossible in a droplet detector due to the low transparency of the gel).

The PICO experiment [232] — the successor to the PICASSO and COUPP experiments — combined the technology of the COUPP's bubble chamber and PICASSO's experience of operating C_3F_8 as a working medium. The choice of C_3F_8 instead of CF_3I was due to a higher bubble nucleation efficiency, better sensitivity in the spin-dependent sector owing to a higher fluorine concentration, and a lower energy threshold for background electrons and gamma quanta. The results of the PICO experiment establish strict constraints on the cross section of WIMP–proton spin-dependent interactions of 3.4×10^{-41} cm^2 with a recoil energy lower than 50 GeV/c^2 for a WIMP mass of 30 GeV/c^2 [233].

The results of the PICASSO, COUPP, and PICO experiments demonstrated a high efficiency of the superheated liquid technique, both for spin-dependent and spin-independent WIMP interactions in the region of low masses. The next stage of collaboration is the PICO-250L experiment with a bubble chamber for 250 kg C_3F_8 [234], which will have a spin-dependent sensitivity to the proton coupling at the level of liquid xenon detectors (Fig. 16).

4.2.7 WIMP directional detectors. Registration of DM-particle motion direction is a new strategy, to which many DM direct search experiments are oriented in the development of next-generation detectors. This strategy, based on the expected anisotropy of DM signals, offers a unique possibility of reliably identifying WIMP interactions, even with unavoidable background events present [128].

The main task of a directional detector is both to measure released energy and to reconstruct the direction of recoil nucleus motion after WIMP scattering, unlike other direct registration detectors, which usually measure only the (time-dependent) energy spectrum. The direction of recoil nucleus motion can be determined by two methods: by totally reconstructing the 3D track of the recoil nucleus (or the projection of the track along one or two dimensions) or by using a detector with an anisotropic response to the direction of recoil nucleus motion, without reconstructing the track itself.

An ideal directional detector should possess the ability to reconstruct the recoil nucleus track in three dimensions with high spatial and angular resolution. It should also be sensitive to the direction of the motion vector, i.e., should determine the beginning and end of a track and not only measure its slope in the space of the detector coordinates. The data collection system of the detector should be radiopure and be able to determine the absolute coordinates of the interaction point inside the active volume of the detector, thereby enabling exclusion of events occurring in the immediate vicinity of the walls and other potentially radioactive components of the detector. A more exact determination of the type of interaction, in addition to the analysis of the direction of motion, may be the analysis of the topology of a reconstructed track [235]. To date, none of the developed technologies has fully satisfied all these requirements.

For a reliable reconstruction of the recoil nucleus track, the detector should provide a high spatial resolution within a sufficiently large volume over a long time period, maximally use radiopure materials, and be inexpensive to produce and simple to operate. These requirements present a number of serious technological challenges, described below.

High spatial resolution. To reconstruct recoil nucleus tracks, the spatial resolution of the detector should not exceed the track length, which, in turn, depends on transferred energy and target material density. For instance, the track length of a recoil nucleus with an energy of 100 keV in a solid body is a mere 100 nm. (Currently, this resolution is achievable only by means of nuclear emulsions.) Most experiments prefer to use as targets rarefied gas (~ 0.1 atm), where recoil nucleus tracks are about a millimeter long. The use of rarefied gases noticeably decreases the requirements for detector spatial resolution, albeit at the expense of the detector's specific mass reduction per unit volume.

Complete 3D event reconstruction. Most detector information readout technologies are not capable of simultaneous high-accuracy measurements of all three coordinates. For this reason, experiments often combine several data-readout technologies for a 3D reconstruction of an event. For instance, the x and y coordinates can be obtained by projecting the signal on a segmented flat sensor, and the z coordinate, by analyzing the temporal component of the signal. Also important is knowledge of the interaction point inside the detector's active volume, which is required to rule out events occurring in the immediate vicinity of potentially radioactive detector components. The measurement of the absolute coordinates can also require the use of additional techniques and methods, e.g., the use of gas mixtures, upon the ionization of which ions with different drift velocities are formed.

Determination of the direction vector. The determination of the points of the beginning and end of the recoil-nucleus motion trajectory is an important measured interaction parameter. Thus, for a reliable identification of a signal from a WIMP with a mass of 100 GeV$/c^2$, a 3D detector would require an exposure lower by an order if, in addition, it is capable of determining the motion vector [236]. For 2D detectors, this difference would make two orders of magnitude. However, for light WIMPs (~ 10 GeV$/c^2$), the determination of the direction vector does not really affect the sensitivity of the detector [129]. The direction vector can be determined in two ways: first, the ionization produced by recoil nuclei changes as they are slowed down and, as a consequence, as does the distribution of induced charge density along the track; second, as recoil nuclei are slowed down, the probability of their scattering to larger angles increases; therefore, the extent of curvature of the track should increase from beginning to end [237]. Both methods require an extremely high spatial resolution, and the former also requires that the ionization along the track be measured.

Determination of the direction of low-energy nuclei. To reveal the interaction of a WIMP with a detector's substance, it is sufficient to register the release of energy inside the active volume, exceeding the detection threshold, the way it is done in numerous direct search experiments. However, as a rule, information about the track geometry is unavailable at minimal energies lower than the direction determination threshold. For WIMP direction-sensitive experiments, it is this threshold that is of major importance and requires considerable effort to reduce it.

Scalability. An obvious problem of (especially gas) detectors is the need for an increase in their size to achieve the required mass of the active substance at reasonable expenses, preserved stability, and possible reconstruction of track parameters.

Moving on to a survey of experiments, detectors can be divided into two groups according to their operating principles: track detectors and anisotropic response detectors. Track detectors have a sufficiently high spatial resolution enabling the complete reconstruction of the recoil nucleus track or its projection, both with and without the determination of the motion vector. In a vast majority of cases, these are experiments with rarefied gas detectors (D^3 (Directional Dark matter Detector) [238], DMTPC (Dark Matter Time Projection Chamber) [239], DRIFT [240], MIMAC [241], NEWAGE [242]), except the NEWSdm experiment [243], which uses a special type of nuclear photoemulsion. Anisotropic detectors are not capable of reconstructing tracks, but the value of the response of these detectors depends on recoil nucleus motion inside the active substance (ADAMO (Anisotropic detectors for DArk Matter Observation) [244], DCaNT (Directionality with Carbon Nano Tubes) [245], columnar recombination in argon and xenon [246]). Thus, by analyzing the response, one can get to know the angle of the track with some discriminated direction inside the detector (electric field vector, crystal axis, or nanotube axis).

Rarefied gas track detectors. Gas detectors are the most widespread among directional DM detection experiments, due to their requirements for spatial resolution being the least strict. Besides, the efficiency and reliability of many gas gain and signal readout technologies used have been brought to perfection under CERN extreme experimental conditions (multiwire chambers [247], MICROMEGAS (MICRO-MEsh-GAseous Structure) [248], GEM (Gas Electron Multipliers) [249], ATLAS Front-End pixel chips [250]). Gas detectors usually use a time-projection chamber (TPC) with gas gain and a data readout system providing a spatial resolution better than 1 mm in one, two, or three dimensions, which makes it possible to partially or completely reconstruct the geometry of the recoil nucleus track. An important technological problem for the TPC is to create large-volume detectors ($\sim 10^3$ m^3) with high spatial resolution and high radiopurity.

Upon the scattering of WIMPs, the recoil nucleus creates in the gas not more than $10^2 - 10^3$ primary electron–ion pairs. Such a weak primary ionization is due to not only a small nucleus recoil energy but also a small gas quenching factor. An estimate for a WIMP with a mass of 100 GeV$/c^2$ moving at a velocity of $10^{-3}\,c$ and coming into a detector filled with CF_4 gas after scattering on a fluorine nucleus yields a maximum energy of 40 keV$_r$. At this energy, the quenching factor is 0.45 [251] and, thus, the electron-equivalent recoil energy is 18 keV$_{ee}$. As a result, the mean energy required to ionize a molecule of CF_4 gas is 34.3 eV [252] and, because of WIMP scattering, 530 electron–ion pairs will only be created.

Registration of such a weak signal requires the use of an electron gain device. The geometry of such devices can be different, but they always have regions of a strong electric field, where primary electrons are accelerated to energies sufficient for shock ionization of surrounding gas molecules. This leads to an exponential growth of ionization electrons, an avalanche. Usually, a multiwire proportional chamber (MWPC, the DRIFT experiment) and relatively recent micropattern gas detectors (MPGDs), such as MICROMEGAS (the MIMAC experiment), GEM (the D^3 and DMTPC experiments), and μPIC (the NEWAGE experiment) are used as a gain device. The MPGDs form an accelerating electric field using screen-printed electrodes, which have much in common with printed

circuit boards. The use of MPGDs provides a high granularity of readout with a relative simplicity of design and fabrication. The electric signal is read out either from a gain electrode (in MWPC, MICROMEGAS, and μPIC) or else using separate sensitive electrodes (in GEM). In addition, in some gases, the process of an avalanche gain can be accompanied by a strong local scintillation of gas molecules, the light from which can be projected onto an optical sensor using a system of lenses through a transparent window in the detector wall (the DMTPC experiment). A detailed review of readout systems for gas detectors is given in [253].

The goal of the joint experiment D^3 of the University of Hawaii (USA) and Lawrence Berkeley National Laboratory (USA) is to develop a detector sensitive to the direction of WIMPs. It is assumed that the future detector will have a volume of the order of 1 m^3. To date, a prototype D^3-Micro has been developed and tested; it represents a TPC filled with a gas mixture of Ar:CO_2 (70:30) or He:CO_2 (70:30). Primary electrons move in a homogeneous electric field of the drift space until they reach the cascade of two GEMs, which amplify ($10^3 - 10^5$ times) the signal projected onto a pixel chip. To increase the effective area of each pixel, a thin layer of metal is applied to the chip. Calibration measurements with the gas mixture at an atmospheric pressure showed the prototype to be able to successfully perform a three-dimensional reconstruction of CR particles, alpha-particles, and recoil nuclei from neutrons to measure the track ionization gradient [254].

Figure 17 shows a schematic of a detector representing a TPC with an active volume of $30 \times 30 \times 41$ cm^3, filled with CF_4 gas under a pressure of 0.1 atm. The primary electron signal is amplified in the GEM, and the signal readout is performed using a μ-PIC micropixel chamber. The energy threshold for determining the direction is 50 keV_{ee}; angular resolution is 40°; and registration efficiency of recoil nuclei and electrons is 0.4 and 2.5×10^{-5}, respectively. In 2015, the D^3 collaboration published the results of an exposure equivalent to 0.327 kg day, where a value of 5.57×10^{-34} cm^2 for a WIMP with a mass of 200 GeV/c^2 was achieved. Since that time, the collaboration has accumulated about 200 more days of exposure, bringing it to 2.385 kg day; supplemented data are in the processing stage [255].

The DRIFT collaboration was one of the first to begin using rarefied gas for the directional search for signals in DM particle scattering [240]. The DRIFT-IId detector is located in the Boulby underground laboratory. As is shown in Fig. 18, the detector consists of two opposite TPCs with a common cathode and total volume of about 1 m^3. The readout is by means of two MWPCs on opposite sides of the detector. To decrease diffusion, a $CF_4 : CS_2 : O_2$ mixture is used, with the addition of negative CS_2, whose ions are the main carriers of charge to the readout MWPCs. An insignificant addition of one more electronegative gas, oxygen, introduces into the gas mixture ions at drift rates distinct from CS_2^-, which makes possible the use of the minority carrier method to measure the absolute coordinate z [256, 257]. According to the method, the distance from an event to the readout plane is directly proportional to the time interval between the registration of the signal for the arrival of minority carriers and main carriers of charge. The direction of the motion vector is determined through the measurement of the density gradient of the ionization charge along the track trajectory.

A considerable concentration of fluorine as a component of CF_4 in the gas mixture enabled the DRIFT experiment to

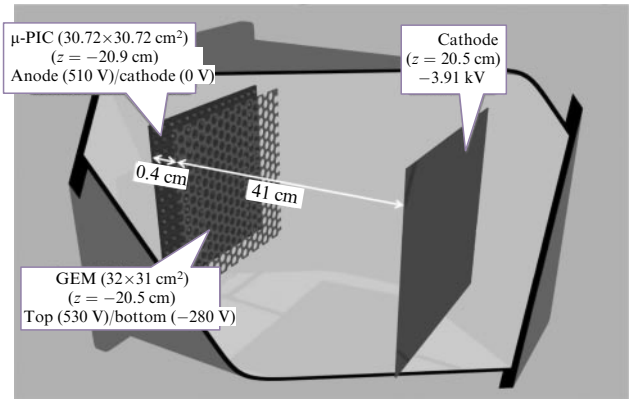

Figure 17. Detector consisting of a μ-TPC, gas recirculation system, and readout electronics. Schematic of the μ-TPC: drift chamber, μ-PIC, and GEM. Active volume of detector is $30.72 \times 30.72 \times 41$ cm^3. (Adapted figure from [255].)

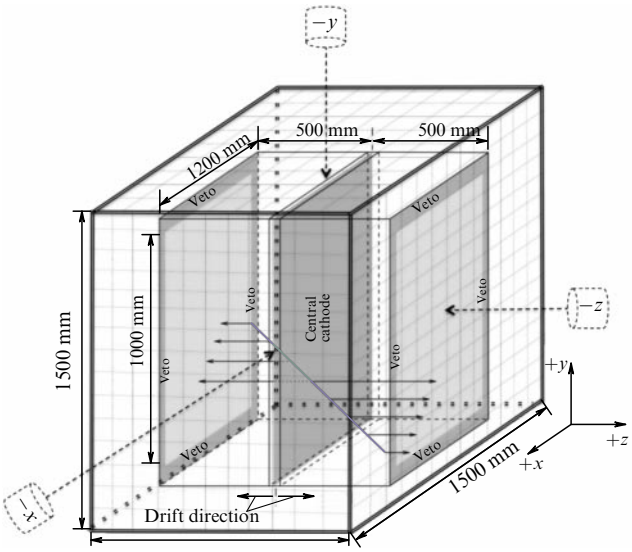

Figure 18. Schematic of DRIFT-IId detector showing central cathode, readout MWPC with designated veto zones, directions of drift, vacuum container, etc. Anode wires of the MWPC are parallel to the y-axis, net wires are parallel to the x-axis, and drift field is parallel to the z-axis [258].

study the spin-dependent cross section of WIMP interaction. In 2017, the collaboration published a result constraining the cross section to 2.8×10^{-37} cm^2 for a WIMP with a mass of 100 GeV/c^2. To date, this is the best result among experiments with directional detectors.

The detector of the DMTPC experiment represents a four-chamber TPC about 1 m^3 in volume, filled with CF_4 gas at a pressure of 30–75 mm Hg, in which each pair of chambers has a common anode. A high-quality image of the anode is projected by an optical system through a transparent window on the closest end wall of the chamber onto a CCD camera sensor. In early prototypes, electron amplification was by means of a GEM cascade, but in later detectors, to provide better visibility, they were replaced by thin wire nets. The transparent anode enables the CCD camera 'to see' the scintillation light on both sides of it, so that one CCD camera simultaneously registers events from both TPCs adjacent to the common anode. In order to measure the time constituent of the signal and to trigger the CCD cameras, the detector is equipped with several MPTs; to measure the energy (in

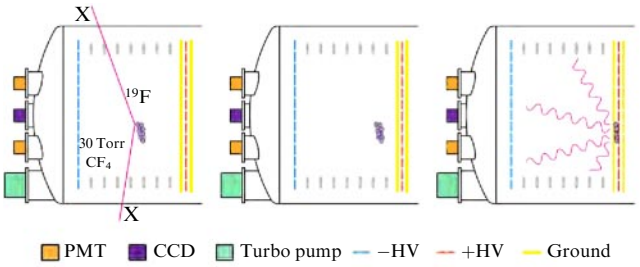

Figure 19. (Color online.) Illustration of the operating principle of DMTPC detector [259]. +HV and −HV, high-voltage positive and negative electrodes.

addition to the CCD cameras), the signal from sensitive electrodes is analyzed. The event registration principle is shown in Fig. 19.

Optical readouts using CCD cameras significantly simplifies data collection. Moreover, it requires no direct contact with the anode, thereby minimizing the number of potentially radioactive materials in contact with the active substance of the detector. One of the drawbacks of the approach is that the measurements are limited to only the 2D projection of the track; however, at present, the potential to produce the third coordinate by signals from MPTs or sensitive electrodes is being studied [260]. According to the calibration data, the detection/direction/vector-determination thresholds are equal, respectively, to 25 keV_r, 40 keV_r, and 55 keV_r at a pressure of 100 mm Hg, and the energy and angular resolution are, respectively, 15% and 40° at 80 keV_r [257].

Figure 20 presents the published results of WIMP searches by the DMTPC, DRIFT, and NEWAGE experiments with directional gas detectors compared with other DM direct-search experiments.

Solid-state track detectors. The spatial resolution of the order of several hundred nanometers required for recoil track registration is unachievable for most modern detector technologies. The only exception is nuclear emulsion.

The NEWSdm collaboration [243] developed at the Gran Sasso underground laboratory uses an alternative approach to the construction of a scalable WIMP direction-sensitive detector based on new-type (NIT, Nano-Imaging Tracker) nuclear emulsions. These high-granularity nuclear emulsions were developed in 2010 at Nagoya University (Japan) [262].

The nuclear emulsion consists of minute (several ten to several hundred nanometers) silver bromide (AgBr) crystals uniformly distributed in the bulk of the polymer, as a rule, gelatine. AgBr crystals are semiconductors with a forbidden band width of 2.7 eV and play the role of sensors. The signal registration mechanism in the nuclear emulsion is illustrated in Fig. 21. Ionization electrons formed during the passage of a charged particle through a crystal migrating inside it reduce one of the silver ions, which becomes the center of metal-silver cluster formation owing to the reactions

$$Ag^+ + e^- \to Ag_1\,, \tag{13}$$

$$Ag_1 + Ag^+ + e^- \to Ag_2\,, \tag{14}$$

$$\ldots\,, \tag{15}$$

$$Ag_{(n-1)} + Ag^+ + e^- \to Ag_n\,. \tag{16}$$

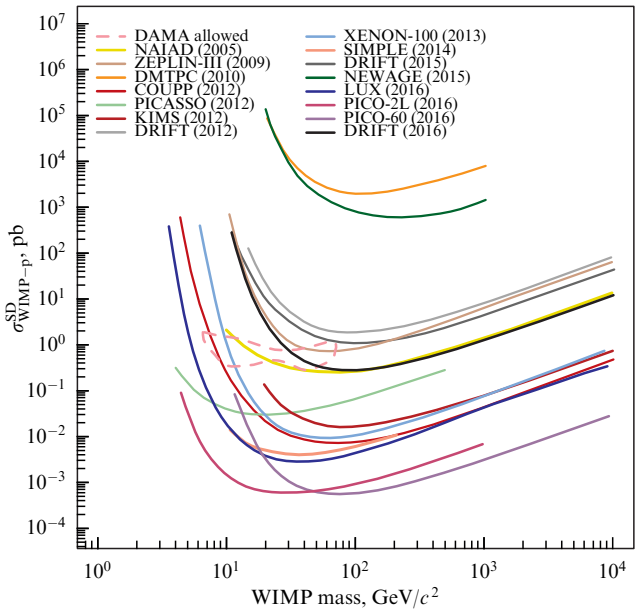

Figure 20. (Color online.) 90% confidence upper limits for the WIMP–proton spin-dependent cross section as a function of the mass [261].

At $n \geqslant 4$, this cluster becomes the stable center of a hidden image and can be preserved in emulsion for a long time (several years). In the process of a special chemical treatment (development) of the emulsion, the hidden image centers transform into metal silver grains, whose size and shape can be adjusted by the development conditions.

After development, the trace of a charged particle in nuclear emulsion looks like a chain of metal silver grains. The mean distance between grains is about 71 nm, and it is an inner threshold for a minimally allowed track length, which in the case of scattering on a carbon nucleus corresponds to a recoil energy of about 25 keV. The average size of AgBr crystals in NIT emulsion is 40 nm, and grains after development have an extended shape of an average size of about 40 nm, too [262]. The new generation of NIT emulsions, Ultra-NIT, with a crystal size of 20 nm, will enable decreasing these thresholds to 40 nm and 13 keV, respectively [262].

Although the density of NIT emulsion is sufficiently high (3.44 g cm^{-3}), and a relatively small volume is required to achieve large masses, the readout of information with the required spatial resolution from the entire volume of the detector is a rather complex technological task. First and foremost, this is because the resolution of fast optical microscopes is restricted by diffraction and does not exceed 200 nm, and alternative readout techniques, such as X-ray or electron microscopy, are too slow. For this reason, the readout of information from emulsion plates is performed by various types of optical microscopes in several stages:

(1) Fast scanning of the entire volume of emulsion with robotic microscopes. For this, optical microscopes and fast scanning technologies developed for the OPERA experiment are used [37, 264, 265]. In the process of scanning, the coordinates of all found events are memorized, and tracks longer than several microns are reconstructed and excluded. The achieved scanning rate is 3.25 g h^{-1} [266]; work to further increase it is in progress [267].

(2) Selected events are examined in optical microscopes with resolutions close to the diffraction limit [268], and the forms of event images are analyzed [269]. Although closely

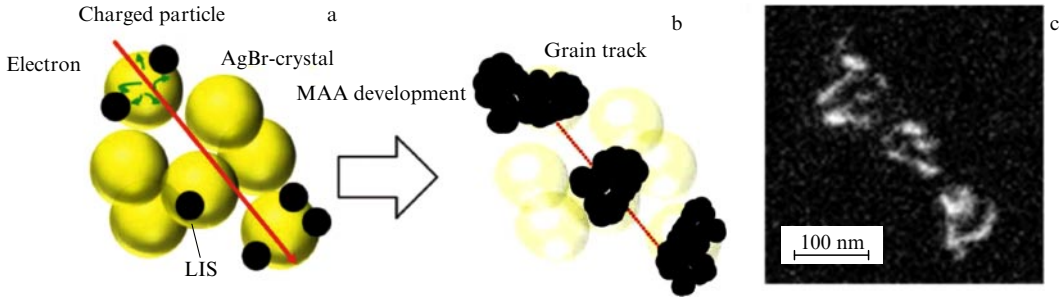

Figure 21. (Color online.) Diagram of the mechanism of signal registration in emulsion. (a) Formation of hidden images. LIS (Latent Image Speck), the centre of a hidden image; MAA (Metol Ascorbic Acid), developer. (b) Metal silver grains after development. (c) Electron microscope image of a track from a carbon ion with energy of 100 keV after development. Upper part of grains is seen, because the depth of the electron-microscope field of vision is about 20 nm [263].

located grains in a track are not resolved in an optical microscope, it is seen from images in Fig. 22 that the presence of several grains is reliably revealed by the shape of the track image: the image of a single grain has an ideally round shape, whereas that of a track (two or more grains) has the form of an ellipse, the major axis of which is co-directed with the track. Analysis of the form of the image makes it possible to rule out events with too round or large and irregular a shape.

(3) Selected events are analyzed on the super-high resolution optical microscope created at the University of Naples (Italy) [270]. The basis of the SRPIM super-resolving method (Super-Resolution Plasmon Imaging Microscopy) [263] developed by the NEWSdm collaboration is the phenomenon of plasmon resonance on the surface of metal silver grains. The dependence of the cross section of light scattering by grains several ten nanometers in size greatly depends on the wavelength and polarization of incident light and has a pronounced resonance peak when the electric field frequency of the wave coincides with the frequency of electronic cloud oscillation. Analysis of the distribution of scattered light intensity enables performing the reconstruction and measurement of the track parameters.

(4) Candidate events undergo a check with X-ray or electron microscopes.

Multistage information readout enables processing a detector 1 kg in mass over several months. The possibility of reconstructing tracks of carbon ions with energies of 100 keV [263] and 60 keV [270] with angular resolutions of 17° and 31°, respectively, was demonstrated. A specialized microscope for high-accuracy measurements along the optical axis of the microscope, enabling the analysis of the light scattered by track grains simultaneously in two orthogonal projections, was developed and patented [271].

Measurements of the intrinsic neutron background of NIT emulsion showed it to be unessential up to an exposure of 10 kg year^{-1} [272]. The possibility of replacing gelatine with a synthetic polymer to exclude the radioactive isotope ^{14}C from the composition of the emulsion is being analyzed at present. The properties of NIT emulsion at cryogenic temperatures are also under investigation [273]. Thus, a significant decrease in the probability of spontaneous thermoactivation of AgBr crystals was noted at liquid nitrogen temperatures, as was a sharp reduction in the sensitivity of the emulsion to gamma radiation and electrons while preserving a sufficient sensitivity to recoil nuclei. Specialized artificial neuronal networks and machine learning algorithms are being developed to determine the type of scattering (electron or nuclear) [274].

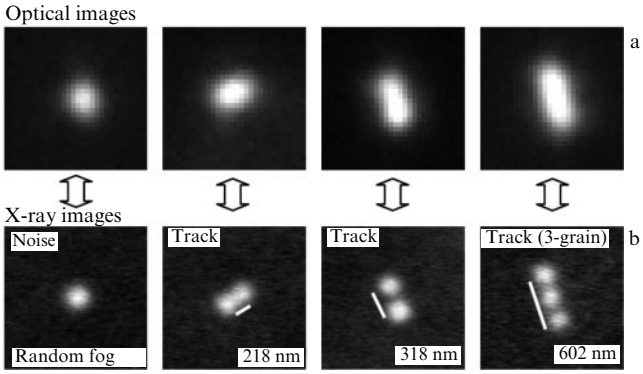

Figure 22. Images of the same events in NIT using an optical microscope (a) and an X-ray microscope (b) [243].

To demonstrate the scalability of the emulsion technology, the collaboration is developing a prototype of a detector 1 kg in mass (see Fig. 23). As the emulsion possesses no spatial resolution, it is necessary to maintain a constant orientation of the detector with respect to the WIMP flux during the entire time of exposure. For this, the detector will be mounted on an equatorial telescope compensating for the revolution of Earth. According to the simulation results shown in Fig. 24a, over a year of exposure, it could be possible to rule out the greater part of the parameter space constrained by the DAMA/LIBRA experiment, even without using information about the direction. By the estimates shown in Fig. 24b, an emulsion detector with a mass of 10 tons and a reconstruction threshold of 30 nm is able to reach the neutrino limit over a year of operation [130].

Anisotropic response detectors. To determine the direction of WIMPs, anisotropic detectors do not rely on the reconstruction of the track geometry, but on a detector property sensitive to the direction of motion of the recoil nucleus. As a rule, in this way it becomes possible to measure the angle between the direction of the track and some designated direction inside the detector, and in some cases also to determine the direction of the track motion vector.

The ADAMO experiment [244] was proposed by participants of the DAMA experiment as the realization of the possibility of expanding the detection technology by adding a WIMP direction-sensitive element. The sensitive element of the detector will be anisotropic $ZnWO_4$ inorganic crystals, the main property of which is a dissimilar scintillation response for different directions of heavy ion motion with respect to the crystal axes. Experiments with α-particles demonstrated a

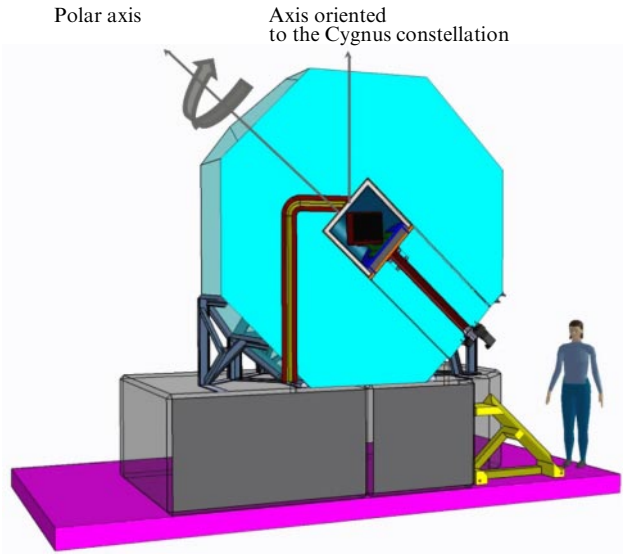

Figure 23. Setup of the NEWSdm experiment [275]. Emulsion module is arranged on the equatorial telescope inside a 1-m-thick polyethylene protective capsule.

1.5-fold difference in quenching factors between the major and minor axes. At the same time, experiments with electrons show the isotropy of scintillation. It is expected that these properties of the crystal will also be preserved for ions of lesser energies and will enable an effective discrimination of electron and ion events. The experiment assumes the production of 200 kg of low-radioactive crystals and their installation and exposure over a period of 5 years in the Gran Sasso underground laboratory [276]. The axes of the crystals with the largest longitudinal quenching factor will be directed vertically upwards; those with the smallest factor, to the north. At the latitude of Gran Sasso, these directions correspond almost exactly to the direction towards the Cygnus constellation, i.e., the expected 'WIMP wind' direction, with a difference of 12 h. In this way, the daily modulation of detector's sensitivity and, as a consequence, the modulation of the signal registration rate in the detector, could be maximized. An additional direction-sensitive parameter is the shape of the scintillation pulse, which also depends on the direction of ion motion with respect to the crystal axes. As expected, its shape will also change with a periodicity of 24 h, which, together with the synchronous change in the event registration rate, will be convincing proof of the galactic origin of the registered particles.

The DCaNT experiment [245] proposes the use of the effect of channelling in carbon nanotubes. Upon interaction of a WIMP with the material of a nanotube, the recoil nucleus may turn out to be 'knocked out' from the nanotube wall into an internal channel. In this regard, if the kinetic energy, corresponding to the projection of a recoil nucleus pulse to the plane perpendicular to the axis of the nanotube, is smaller than the potential Coulomb barrier (~ 400 eV), its reflection occurs. Furthermore, the longitudinal component of the velocity remains invariable, and the recoil nucleus reaches one of the ends of the nanotube practically without energy losses and can be registered there. Evidently, the probability of channelling strongly depends on the direction of incidence of the WIMP and is maximal if it is incident along the axis of the nanotube and the recoil nucleus is scattered forward.

Figure 25a shows the detector concept proposed by the DCaNT experiment [277]. The detector consists of a double brush of nanotubes applied on both sides of the substrate. To register recoil nuclei escaping the open ends of the nanotubes, the substrate with nanotubes is placed into a gas TPC with an electric field directed perpendicular to the nanotube axes, gas amplification, and a readout device that measures the energy of the recoil nucleus and direction of its motion. To ensure the co-directivity of the nanotube axes with the direction of the 'WIMP wind', the detector is assumed to be mounted on an equatorial telescope. The exceedance of the number of ions escaping the nanotube brush at the back surface of the substrate compared with the front surface (whose recoil nuclei are absorbed by the substrate) will be a signal of the registration of DM particles. It is assumed that the detector will comprise 100 panels 1×1 m^2 in area with a nanotube brush applied on both surfaces, and a total mass of carbon

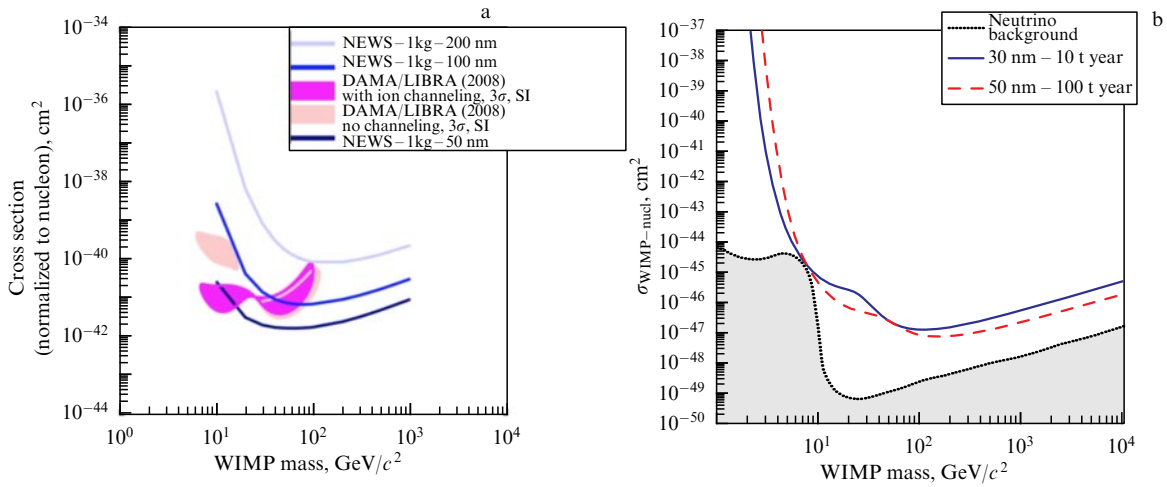

Figure 24. (Color online.) (a) 90% confidence upper limits for a NIT detector with an exposure of 1 kg year and different reconstruction thresholds varying from 200 nm to 50 nm; zero-background hypothesis was used, without the use of information about the direction [243]. (b) Upper limit for the NEWSdm detector is shown for exposures of 10 t year (solid blue curve) and 100 t year (red dashed curve) with sensitivity thresholds of 30 nm and 50 nm, respectively. Black dashed curve represents neutrino limit [130].

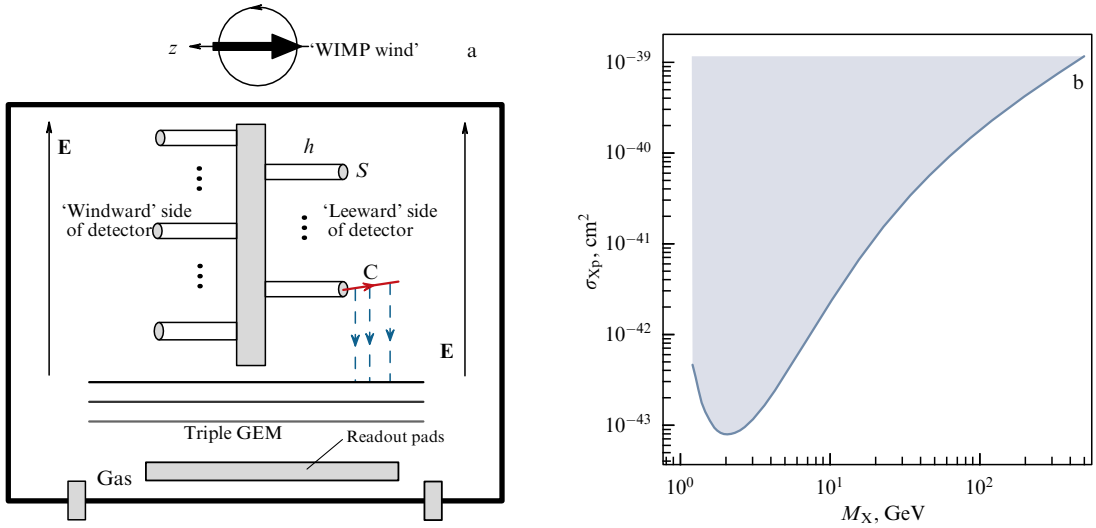

Figure 25. (a) Schematic of a detector with a double brush of nanotubes of length $h = 100-200$ μm and cross section S of diameter ~ 10 nm. Ionization electrons produced by ion C escaping nanotube drift in electric field E towards the GEM. Substrate is 1 mm thick and has an area of 10×10 cm^2 [277]. (b) 90% confidence upper limit for WIMP scattering cross section, σ_{Xp}, calculated for a detector 10 kg in mass and 3-year exposure [278].

nanotubes of 10 kg. The results of calculations of the sensitivity of this detector to WIMP interactions over a three-year exposure are given in Fig. 25b.

Experiments using columnar recombination in noble gases and liquids. Taking into account the effect of columnar recombination in future detectors based on liquefied noble gases can make them sensitive to WIMP direction. An ionization trace from a recoil nucleus can be represented as a continuous cloud of ions and electrons extended along the trace, the so-called ionization column. Immediately after thermalization, ions and electrons begin to drift in an external electric field. If the field is perpendicular to the ionization column, the electrons and ions, moving in different directions, will drift apart almost immediately. If the field and the column are co-directed, then, contrariwise, most ions and electrons will drift on opposite courses, experiencing more collisions and, as a consequence, recombinations. Thus, the ratio of the value of recombination to ionization can serve as a measure of the angle between the recoil nucleus direction of motion and the direction of the electric field in the detector.

Initially, this method was proposed to be used in detectors based on gaseous xenon at a pressure of 10 atm [279]. The density of xenon at this pressure equals 0.05 g cm^{-3}, which is approximately two orders of magnitude greater than the density of the gas in gas trackers. The capture of an electron by an ion occurs when the distance between them is smaller than the so-called Onsager radius, determined as the distance r_0 at which the potential energy of the pair equals the kinetic energy of electron E, or $r_0 \equiv e^2/(\varepsilon E)$, where ε is the dielectric permeability of the medium. For instance, for the thermal electron ($E = k_B T$, where k_B is the Boltzmann constant) in gaseous xenon, $r_0 \approx 70$ nm, whereas in liquid xenon, it decreases to 54 nm. For comparison, the track length of the recoil nucleus with an energy of 30 keV is ~ 2100 nm and ~ 35 nm in gaseous and liquid xenon, respectively. The track length of the recoil nucleus in liquid xenon is significantly smaller than the Onsager radius, which makes impossible the use of the columnar recombination technique to impart WIMP directional sensitivity to modern and future experiments with LXe-TPC, such as XENON, LUX, and DARWIN.

In contrast, in liquid argon, the track length of the recoil nucleus exceeds the Onsager radius (~ 80 nm) at energies of the order of 35 keV. The SCENE (SCintillation Efficiency of Noble Elements) experiment demonstrated an insignificant anisotropy of LAr-TPC scintillation response for recoil nuclei with an energy of 57.3 keV [280]. The possibility of using the columnar recombination technique in LAr-TPC detectors has been studied by the DarkSide experiment and is expected to be applied in the DarkSide-20k detector [189].

5. Conclusion. Some results from and prospects for the search for weakly interacting massive dark matter particles

The search for DM particles and the determination of their properties are some of the major issues of modern physics. Astronomical data provided experimental evidence for the existence of a hidden mass in the Universe, which enabled establishing the actuality of the existence of DM and localizing regions of its clustering but gave no information on what it consists of. It is assumed that the properties of DM particle carriers are consistent with Universe evolution models and should not contradict the existing Standard Model of elementary particles, which describes most physical data observed. According to modern views, DM particles have nonzero masses (are involved in gravitational interactions with baryonic matter) and presumably may experience weak interactions. The masses of the possible candidates theoretically range from 10^{-21} eV up to 10^{19} GeV. As DM particles are barely involved in electromagnetic interactions, they should be electrically neutral, though there are models that concede small charges lesser than $10^{-3}e$ in them. The most actively considered candidates are weakly interacting massive particles of dark energy, WIMPs, which are involved in the gravitational interaction and interact with W and Z bosons.

An indirect search for signals from DM particles is possible by registering products of their annihilation or decay in galactic gamma radiation, neutrino fluxes, and charged particles of high-energy cosmic rays. Rather significant results, from the viewpoint of DM signal studies, have been obtained in this field of research using the LAT telescope, the main detector of the FGST, successfully operated in space for the 12th (!) year now. The Fermi-LAT collaboration revealed a source of gamma radiation in the Milky Way galactic center with gamma quantum energy exceeding the energy of hard X-ray radiation by two–three orders of magnitude. The gamma spectrum of the radiation agrees with DM particle masses from 10 GeV to 1 TeV, annihilating into quarks b and $\bar{\text{b}}$, and masses from 10 GeV to 30 GeV, annihilating into τ^+- and τ^--leptons.

Ground-based Cherenkov gamma telescopes are instruments with far greater registration areas than space-based telescopes. Four gamma telescopes — HESS, MAGIC, FACT, and VERITAS — are operating at present, the results of the work of which researchers have used to succeed in establishing the boundaries of DM particle masses and upper limits of WIMP annihilation velocities for various channels. The obtained lower estimate for the mass of WIMP cold dark matter heavy particles from the data of these facilities is several hundred GeV.

It is assumed that DM particles from the galactic halo, when passing through astrophysical objects (including the Sun and Earth) are trapped by their gravitational fields, which can be evidenced by the annihilation products of these particles registered in cosmic radiation, in particular, neutrinos whose energies exceed by several orders of magnitude the energies of neutrinos formed in nuclear reactions (tens and hundreds of GeV against several MeV). They can be registered in observations in the direction of the Sun or the center of Earth performed, in particular, by the Super-Kamiokande, ANTARES, and IceCube neutrino telescopes. The registration of several ten events from ultrahigh-energy neutrinos in the range of $\geqslant 1$ PeV in the IceCube experiment, which can be indicative of the existence of high-energy neutrinos, possibly from DM, can be considered to be the most significant contribution to neutrino astrophysics.

Direct detection of DM particles is based on the registration of recoil nuclei under elastic scattering of WIMPs on target nuclei. Due to the small cross section of interaction of DM particles with matter, experiments for their search by direct methods have one common feature: they are carried out in underground laboratories so as to significantly reduce the influence of the background. One of the largest experiments on the direct registration of DM particles, DAMA/LIBRA, being performed at present and providing a strict selection of signal events, a multilevel isolation of the background, and continuous control of residual radioactivity, communicated the registration of weak annual oscillations of signals from DM with an amplitude of about 1–2% with a confidence of 12.9σ. This result, albeit using fewer statistics, was confirmed by the CoGeNT experiment. However, another direct WIMP detection experiment, COSINE-100, also operated with scintillators, did not confirm the presence of features of signal exceedance over the expected background. The results of the COSINE-100 experiment rule out with a 90% confidence spin-independent WIMP–nucleon interactions as a cause of annual modulation observed by the DAMA collaboration. Similarly, the results of 4.2 years of operation the CDEX-1 semiconductor detector excluded the conclusions of the DAMA/LIBRA and CoGeNT experiments with a confidence of 99.99% and 98.0%, respectively.

The semiconductor detectors used in direct DM registration experiments, despite their high sensitivity, have not yet been able to provide unambiguous and convincing evidence of DM existence. One of the explanations is that WIMPs may be lighter than assumed and that the energy which recoil nuclei can release in the detector is lower than the thresholds achieved in these experiments. As a result, interest in facilities with lower thresholds for recoil nuclei has emerged, in particular, in cryogenic bolometers.

In the context of the search for DM, the technology of superheated liquids implemented in the form of bubble chambers and droplet detectors has returned to experimental physics, demonstrating a high efficiency of the method of superheated liquid for both spin-dependent and spin-independent WIMP interactions in the region of low masses.

An efficient basis of large-mass homogeneous and compact scintillation detectors is the liquid-phase noble gases xenon and argon, which are easily ionized during the passage of charged particles. The DEAP collaboration with a liquid argon-based single-phase detector obtained an estimate for the scattering cross section lower limit of 3.9×10^{-45} cm^2 (1.5×10^{-44} cm^2) for WIMPs of 100 GeV/c^2 mass (1 TeV/c^2) with a 90% confidence. To date, this is the record result for the spin-independent WIMP scattering cross section for detectors based on liquid argon. Implementation of the new program for direct DM registration within the DarkSide-20k experiment using a large-mass two-phase time projection chamber based on liquid argon will enable a sensitivity of 1.2×10^{-47} cm^2 for the direct registration of WIMPs at a mass of 1 TeV/c^2. The strictest limitations on the spin-independent WIMP–nucleon scattering cross section were obtained by two-phase time projection chambers using liquid xenon as the active target material. Owing to the scalability of two-phase technology, future multi-ton experiments with liquid xenon detectors are expected to improve the sensitivity to WIMPs by about three orders of magnitude.

The complexity of the task of DM particle detection requires, apart from continuous upgrades of the operational facilities, drastically new approaches to the development of technologies for searching for them. A novel promising strategy is the directional registration of DM particles, to which the direct search experiments are oriented in preparing next-generation detectors. This strategy gives a unique possibility of reliably identifying WIMP interactions even with unavoidable background events present. The best result among the experiments with direction-sensitive detectors obtained in the DRIFT experiment limits the spin-dependent WIMP interaction cross section by a value of up to 2.8×10^{-37} cm^2 for WIMPs with masses of 100 GeV/c^2. We should especially note the original NEWSdm experiment being developed, which not only offers the advanced technology of nano-sized emulsions for searching for DM but also has patented a superhigh-resolution optical microscope for their scans.

Despite the active search for DM carriers and the important estimates obtained, none of the existing experiments can claim their confident detection to date. Promising techniques are being developed, and the most probable regions of the DM particle search are being determined. As V L Ginzburg wrote formulating the most pressing problems of 21st century physics, ''since the nature of dark matter is

absolutely unclear, the solution to this problem may now be thought of as the most important in astronomy" [281]. A diversity of experimental methods for registering DM particle carriers, major results from the search for them obtained to date, and original technologies and instruments being developed open enticing prospects for the proof of the existence of DM and the solution to topical problems in New Physics.

This research was funded by the Russian Foundation for Basic Research within the framework of the scientific project no. 19-12-50184.

References

1. Spergel D N *Science* **347** 1100 (2015)
2. Grebenikov E A, Ryabov Yu A *Poiski i Otkrytiya Planet* (Searching for and Discovering Planets) 2nd ed. (Moscow: Nauka, 1984)
3. Bessel F W *Mon. Not. R. Astron. Soc.* **6** 136 (1844)
4. Zasov A V et al. *Phys. Usp.* **60** 3 (2017); *Usp. Fiz. Nauk* **187** 3 (2017)
5. Wechsler R H, Tinker J L *Annu. Rev. Astron. Astrophys.* **56** 435 (2018); arXiv:1804.03097
6. Zwicky F *Astrophys. J.* **86** 217 (1937)
7. Roszkowski L, Sessolo E M, Trojanowski S *Rep. Prog. Phys.* **81** 066201 (2018); arXiv:1707.06277
8. Boveia A, Doglioni C *Annu. Rev. Nucl. Part. Sci.* **68** 429 (2018)
9. Bertone G, Hooper D, Silk J *Phys. Rep.* **405** 279 (2005)
10. Rubin V C, Ford W K (Jr.), Thonnard N *Astrophys. J.* **238** 471 (1980)
11. Borriello A, Salucci P, Danese L *Mon. Not. R. Astron. Soc.* **341** 1109 (2003); astro-ph/0208268
12. Křížek M, Křížek F, Somer L *Bulg. Astron. J.* **25** 64 (2016)
13. Sofue Y, Rubin V *Annu. Rev. Astron. Astrophys.* **39** 137 (2001)
14. Roberts M S, Rots A H *Astron. Astrophys.* **26** 483 (1973)
15. Battaglia G et al. *Mon. Not. R. Astron. Soc.* **364** 433 (2005)
16. Stewart G C et al. *Astrophys. J.* **278** 536 (1984)
17. Fabricant D, Gorenstein P *Astrophys. J.* **267** 535 (1983)
18. Jeltema T E, Profumo S *Astrophys. J.* **686** 1045 (2008)
19. Pretzl K *Spatium* (7) 3 (2001) http://www.issibern.ch/PDF-Files/Spatium_7.pdf
20. Jee M J et al. *Astrophys. J.* **661** 728 (2007); arXiv:0705.2171
21. Press Release of NASA/ESA HUBBLE Space Telescope. Images: Dark matter ring in galaxy cluster Cl 0024 + 17 (ZwCl 0024 + 1652), https://www.spacetelescope.org/images/heic0709a
22. Ade P A R et al. (Planck Collab.) *Astron. Astrophys.* **594** A13 (2016)
23. Chevalier L, Brun P *PoS EDSU* **2018** 020 (2018)
24. Schumann M *J. Phys. G* **46** 103003 (2019); arXiv:1903.03026
25. Del Nobile E, Nardecchia M, Panci P *JCAP* **2016** (04) 048 (2016)
26. Drees M *PoS ICHEP2018* **340** 730 (2019); arXiv:1811.06406
27. Feng J L *Annu. Rev. Astron. Astrophys.* **48** 495 (2010)
28. Boveia A, Doglioni C *Annu. Rev. Nucl. Part. Sci.* **68** 429 (2018)
29. Klein O *Z. Phys.* **37** 895 (1926)
30. Appelquist T, Cheng H-C, Dobrescu B A *Phys. Rev. D* **62** 035002 (2001); hep-ph/0012100
31. Servant G, Tait T M P *Nucl. Phys. B* **650** 391 (2003)
32. Feng J L, Rajaraman A, Takayama F *Phys. Rev. Lett.* **91** 011302 (2003); hep-ph/0302215
33. Feng J L, Rajaraman A, Takayama F *Phys. Rev. D* **68** 063504 (2003); hep-ph/0306024
34. Feng J L *Annu. Rev. Astron. Astrophys.* **48** 495 (2010)
35. Griest K, in *Encyclopedia of Astronomy and Astrophysics* (Ed. P Murdin) (Bristol: Institute of Physics Publ., 2002) p. 2634
36. Tisserand P et al. *Astron. Astrophys.* **469** 387 (2007)
37. Agafonova N et al. (OPERA Collab.) *Phys. Rev. Lett.* **120** 211801 (2018); arXiv:1804.04912
38. Dodelson S, Widrow L M *Phys. Rev. Lett.* **72** 17 (1994)
39. Boyarsky A, Ruchayskiy O, Shaposhnikov M *Annu. Rev. Nucl. Part. Sci.* **59** 191 (2009); arXiv:0901.0011
40. Seljak U et al. *Phys. Rev. Lett.* **97** 191303 (2006); astro-ph/0602430
41. Viel M et al. *Phys. Rev. Lett.* **97** 071301 (2006); astro-ph/0605706
42. Gell-Mann M, Ramond P, Slansky R *Conf. Proc. C* **790927** 315 (1979); arXiv:1306.4669
43. McDonald J *Phys. Rev. D* **50** 3637 (1994); hep-ph/0702143
44. Holdom B *Phys. Lett. B* **166** 196 (1986)
45. Huang K *Quarks, Leptons and Gauge Fields* (Singapore: World Scientific, 1992) p. 286
46. Zyla P A et al. (Particle Data Group) *Prog. Theor. Exp. Phys.* **2020** 083C01 (2020)
47. Archidiacono M et al. *JCAP* **2013** (10) 020 (2013); arXiv:1307.0615
48. Raffelt G G, in *Axions* (Lecture Notes in Physics, Vol. 741, Eds M Kuster, G Raffelt, B Beltrán) (Berlin: Springer, 2008) p. 51
49. McGaugh S S, Barker M K, de Blok W J G *Astrophys. J.* **584** 566 (2003); astro-ph/0210641
50. Bezrukov F, Chudaykin A, Gorbunov D *JCAP* **2017** (06) 051 (2017); hep-ph/1705.02184
51. Meissner K A, Nicolai H *Phys. Rev. D* **100** 035001 (2019)
52. Akimov D Yu *Instrum. Exp. Tech.* **44** 575 (2001); *Prib. Tekh. Eksp.* (5) 6 (2001)
53. Ryabov V A, Tsarev V A, Tskhovrebov A M *Phys. Usp.* **51** 1091 (2008); *Usp. Fiz. Nauk* **178** 1129 (2008)
54. Bergström L, Bringmann T, Edsjö J *Phys. Rev. D* **83** 045024 (2011)
55. Arrenberg S et al., arXiv:1310.8621
56. Bergström L *Rep. Prog. Phys.* **63** 793 (2000); hep-ph/0002126
57. Cirelli M et al. *JCAP* **2011** (03) 051 (2011); arXiv:1012.4515
58. Kuhlen M, Madau P, Silk J *Science* **325** 970 (2009); arXiv:0907.0005
59. Bertone G et al. *JCAP* **2012** (03) 020 (2012); arXiv:1009.5107
60. Ajello M et al. *Astrophys. J.* **819** 44 (2016); arXiv:1511.02938
61. Atwood W et al. *Astrophys. J.* **697** 1071 (2009); arXiv:0902.1089
62. Abdollahi S et al. *Astrophys. J. Suppl.* **247** 33 (2020)
63. Ackermann M et al. *Astrophys. J.* **840** 43 (2017); arXiv:1704.03910
64. Di Mauro M et al. *Phys. Rev. D* **99** 123027 (2019); arXiv:1904.10977
65. Malyshev D *Nuovo Cimento C* **40** 159 (2017); arXiv:1802.03326
66. Ackermann M et al. (The Fermi-LAT Collab.) *Phys. Rev. Lett.* **115** 231301 (2015); arXiv:1503.02641
67. Abazajian K N, Kaplinghat M *Phys. Rev. D* **86** 083511 (2012)
68. Nolan P L et al. *Astrophys. J. Suppl.* **199** 31 (2012); arXiv:1108.1435
69. Lee S K et al. *Phys. Rev. Lett.* **116** 051103 (2016); arXiv:1506.05124
70. Bartels R, Krishnamurthy S, Weniger C *Phys. Rev. Lett.* **116** 051102 (2016); arXiv:1506.05104
71. Leane R K, Slatyer T R *Phys. Rev. Lett.* **123** 241101 (2019)
72. Coronado-Blázquez J et al. *JCAP* **2019** (11) 045 (2019)
73. Springel V et al. *Nature* **456** 73 (2008)
74. Galper A M, Topchiev N P, Yurkin Yu T *Astron. Rep.* **62** 882 (2018)
75. Cuoco A et al. *Phys. Rev. D* **101** 022002 (2020); arXiv:1912.09373
76. Press W H, Spergel D N *Astrophys. J.* **296** 679 (1985)
77. Bell N F, Petraki K *JCAP* **2011** (04) 003 (2011); arXiv:1102.2958
78. Arina C et al. *Phys. Rev. D* **96** 063010 (2017); arXiv:1703.08087
79. Blennow M, Clementz S, Herrero-Garcia J *Eur. Phys. J. C* **78** 386 (2018)
80. Mazziotta M N *Phys. Rev. D* **98** 022006 (2018); arXiv:1712.07005
81. Ackermann M et al. *Phys. Rev. Lett.* **108** 011103 (2012)
82. Adriani O et al. (Fermi LAT Collab.) *Nature* **458** 607 (2009)
83. Aguilar M et al. (AMS Collab.) *Phys. Rev. Lett.* **122** 041102 (2019)
84. Moskalenko I V, Strong A W *Astrophys. J.* **493** 694 (1998)
85. Delahaye T et al. *Astron. Astrophys.* **524** A51 (2010)
86. Cernuda I *Astropart. Phys.* **34** 59 (2010); arXiv:0905.1653
87. Coutu S *Physics* **6** 40 (2013)
88. Chang J et al. *Astropart. Phys.* **95** 6 (2017); arXiv:1706.08453
89. Ambrosi G et al. (DAMPE Collab.) *Nature* **552** 63 (2017)
90. Abazajian K N, Harding J P *JCAP* **2012** (01) 041 (2012)
91. Abdallah H et al. (H.E.S.S. Collab.) *Phys. Rev. Lett.* **120** 201101 (2018)
92. Aleksić J et al. *JCAP* **2014** (02) 008 (2014); arXiv:1312.1535
93. Anderhub H et al. *JINST* **8** P06008 (2013); arXiv:1304.1710
94. Galante N, VERITAS Collab. *AIP Conf. Proc.* **1505** 202 (2012)
95. Doro M et al. *Astropart. Phys.* **43** 189 (2013); arXiv:1208.5356
96. Hofmann W *The Messenger* (168) 21 (2017)
97. Anastassopoulos V et al. *JINST* **12** P11019 (2017)
98. Ritz S, Seckel D *Nucl. Phys. B* **304** 877 (1988)
99. Markov M A, in *Proc. of the 10th Intern. Conf. on High-Energy Physics, ICHEP 60, Rochester, NY, USA, 25 August – 1 September 1960* (Eds E C G Sudarshan, J H Tinlot, A C Melissinos) (Rochester, NY: Rochester Univ., 1960) p. 578
100. Domogatsky G V, Komar A A, Chudakov A E *Priroda* (3) 22 (1989)
101. Ageron M et al. *Nucl. Instrum. Meth. Phys. Res. A* **656** 11 (2011)
102. Katz U F *Nucl. Instrum. Meth. Phys. Res. A* **567** 457 (2006)

103. Aartsen M G et al. (IceCube Collab.) *JINST* **12** P03012 (2017)
104. Abbasi R et al. *Astropart. Phys.* **35** 615 (2012); arXiv:1109.6096
105. Baur S *PoS ICRC2019* **358** 506 (2020); arXiv:1908.08236
106. Aartsen M G et al. (IceCube Collab.) *Eur. Phys. J. C* **78** 831 (2018)
107. Catena R, Hellström F *JCAP* **2018** (10) 039 (2018)
108. Aartsen M G et al. (IceCube Collab.) *Phys. Rev. Lett.* **113** 101101 (2014); arXiv:1405.5303
109. Esmaili A, Serpico P D *JCAP* **2013** (11) 054 (2013); arXiv:1308.1105
110. Murase K et al. *Phys. Rev. Lett.* **115** 071301 (2015)
111. Aartsen M G et al. (The IceCube Collab.) *PoS ICRC2015* **236** 1081 (2016)
112. Avrorin A D et al. *JETP Lett.* **108** 787 (2018); *Pis'ma Zh. Eksp. Teor. Fiz.* **108** 803 (2018); arXiv:1810.10966
113. Kasen D et al. *Nature* **551** 80 (2017); arXiv:1710.05463
114. Kachulis C et al. (Super-Kamiokande Collab.) *Phys. Rev. Lett.* **120** 221301 (2018); arXiv:1711.05278
115. Frankiewicz K (for the Super-Kamiokande Collab.) *J. Phys. Conf. Ser.* **888** 012210 (2017)
116. Abe K et al. (Hyper-Kamiokande Proto-Collab.), arXiv:1805.04163
117. Kumar J, Sandick P *JCAP* **2015** (06) 035 (2015); arXiv:1502.02091
118. Kozlov A et al. *Nucl. Instrum. Meth. Phys. Res. A* **958** 162239 (2020)
119. Spergel D N *Phys. Rev. D* **37** 1353 (1988)
120. Goodman M W, Witten E *Phys. Rev. D* **31** 3059 (1985)
121. Bertone G (Ed.) *Particle Dark Matter*: *Observations, Models and Searches* (Cambridge: Cambridge Univ. Press, 2010) p. 345
122. Mei D-M, Hime A *Phys. Rev. D* **73** 053004 (2006); astro-ph/0512125
123. Baudis L *Ann. Physik* **528** 74 (2016); arXiv:1509.00869
124. Bozorgnia N, Gelmini G B, Gondolo P *JCAP* **2012** (06) 037 (2012)
125. Bozorgnia N, Gelmini G B, Gondolo P *JCAP* **2012** (08) 011 (2012)
126. Billard J, Mayet F, Santos D *Phys. Rev. D* **82** 055011 (2010)
127. Henderson S, Monroe J, Fisher P *Phys. Rev. D* **78** 015020 (2008)
128. Billard J et al. *Phys. Lett. B* **691** 156 (2010); arXiv:0911.4086
129. Billard J, Mayet F, Santos D *Phys. Rev. D* **85** 035006 (2012)
130. Agafonova N et al. (NEWSdm Collab.) *Eur. Phys. J. C* **78** 578 (2018); arXiv:1705.00613
131. Billard J, Mayet F, Santos D *Phys. Rev. D* **83** 075002 (2011)
132. Lee S K, Peter A H G *JCAP* **2012** (04) 029 (2012); arXiv:1202.5035
133. O'Hare C A J, Green A M *Phys. Rev. D* **90** 123511 (2014)
134. Alves D S M, El Hedri S, Wacker J G *J. High Energ. Phys.* **2016** (03) 149 (2016); arXiv:1204.5487
135. Grothaus P, Fairbairn M, Monroe J *Phys. Rev. D* **90** 055018 (2014)
136. O'Hare C A J et al. *Phys. Rev. D* **92** 063518 (2015); arXiv:1505.08061
137. Irastorza I G, arXiv:0911.2855
138. Bugaev E V et al. *Phys. Rev. D* **58** 054001 (1998); hep-ph/9803488
139. Cheng J-P et al. *Annu. Rev. Nucl. Part. Sci.* **67** 231 (2017)
140. Patrignani C et al. (Particle Data Group) *Chinese Phys. C* **40** 100001 (2016)
141. Hall J *J. Phys. Conf. Ser.* **1468** 012252 (2020)
142. Piquemal F *Eur. Phys. J. Plus* **127** 110 (2012)
143. Votano L *Eur. Phys. J. Plus* **127** 109 (2012)
144. Pandola L *AIP Conf. Proc.* **1338** 12 (2011); arXiv:1102.0208
145. Press Release of Kamioka Observatory, http://www-sk.icrr.u-tokyo.ac.jp/aboutus/index-e.html
146. Fushimi K et al. *J. Phys. Conf. Ser.* **718** 042022 (2016)
147. Press Release of University of Minnesota, http://www.soudan.umn.edu/
148. Bettini A *Eur. Phys. J. Plus* **127** 112 (2012)
149. Kim Y *Bull. Am. Phys. Soc.* **62** Y7.002 (2017)
150. Leo W R *Techniques for Nuclear and Particle Physics Experiments*: *a How-to Approach* (Berlin: Springer, 1994)
151. Shields E, Xu J, Calaprice F *Phys. Procedia* **61** 169 (2015)
152. Park J S et al. *Nucl. Instrum. Meth. Phys. Res. A* **851** 103 (2017)
153. Bernabei R (DAMA Collab.) *Catching Dark Matter Particles in the Galactic Halo with DAMA/LIBRA* (Roma: Aracne Ed., 2019)
154. Bernabei R et al. *Nucl. Instrum. Meth. Phys. Res. A* **592** 297 (2008)
155. Bernabei R *Int. J. Mod. Phys. A* **31** 1642001 (2016)
156. Bernabei R et al. *Nucl. Phys. At. Energy* **19** 307 (2018)
157. Bernabei R et al. *Int. J. Mod. Phys. A* **21** 1445 (2006)
158. Tan A et al. (PandaX-II Collab.) *Phys. Rev. Lett.* **117** 121303 (2016)
159. Aprile E et al. (XENON Collab.) *Phys. Rev. Lett.* **119** 181301 (2017)
160. Agafonova N Yu et al. *Bull. Russ. Acad. Sci. Phys.* **75** 427 (2011); *Izv. Ross. Akad. Nauk Ser. Fiz.* **75** 456 (2011)
161. Amaré J et al. *J. Phys. Conf. Ser.* **1468** 012014 (2020)
162. Adhikari G et al. *Eur. Phys. J. C* **78** 107 (2018); arXiv:1710.05299
163. Prihtiadi H et al. *JINST* **13** T02007 (2018); arXiv:1712.02011
164. Adhikari G et al. (The COSINE-100 Collab.) *Nature* **564** 83 (2018)
165. Lippincott W H et al. *Phys. Rev. C* **86** 015807 (2012)
166. Albert J B et al. (EXO Collab.) *Phys. Rev. C* **89** 015502 (2014)
167. Benetti P et al. *Nucl. Instrum. Meth. Phys. Res. A* **574** 83 (2007)
168. Chepel V, Araújo H *JINST* **8** R04001 (2013); arXiv:1207.2292
169. Hitachi A et al. *Phys. Rev. B* **27** 5279 (1983)
170. Lippincott W H et al. *Phys. Rev. C* **78** 035801 (2008)
171. Lippincott W H et al. *Phys. Rev. C* **81** 039901 (2010)
172. Aalseth C E et al. (The Global Argon Dark Matter Collab.) "Future Dark Matter Searches with Low-Radioactivity Argon", https://indico.cern.ch/event/765096/contributions/3295671/attachments/1785196/2906164/DarkSide-Argo_ESPP_Dec_17_2017.pdf
173. Rielage K et al. *Phys. Procedia* **61** 144 (2015); arXiv:1403.4842
174. Ajaj R et al. (DEAP Collab.) *Phys. Rev. D* **100** 022004 (2019)
175. Abe K et al. (XMASS Collab.) *Phys. Lett. B* **789** 45 (2019)
176. Wang J-J, arXiv:1711.02117
177. Rielage K et al. *Phys. Procedia* **61** 144 (2015); arXiv:1403.4842
178. Aprile E et al. *Astropart. Phys.* **35** 573 (2012); arXiv:1107.2155
179. Aprile E et al. (XENON Collab.) *Phys. Rev. Lett.* **119** 181301 (2017)
180. Cui X et al. (PandaX-II Collab.) *Phys. Rev. Lett.* **119** 181302 (2017)
181. Akerib D S et al. (LUX Collab.) *Phys. Rev. Lett.* **118** 021303 (2017)
182. Akimov D Yu et al. *Astropart. Phys.* **34** 151 (2010); arXiv:1004.4207
183. Aprile E et al. (XENON Collab.) *Phys. Rev. D* **94** 122001 (2016)
184. Xia J et al. *Phys. Lett. B* **792** 193 (2019); arXiv:1807.01936
185. Aprile E et al. (XENON Collab.) *Phys. Rev. Lett.* **121** 111302 (2018)
186. Akerib D S et al. (LUX-ZEPLIN Collab.) *Phys. Rev. D* **101** 052002 (2020)
187. Aalbers J et al. *JCAP* **2016** (11) 017 (2016); arXiv:1606.07001
188. Billard J, Figueroa-Feliciano E, Strigari L *Phys. Rev. D* **89** 023524 (2014); arXiv:1307.5458
189. Input to the European Particle Physics Strategy Update 2018-2020: Future Dark Matter Searches with Low-Radioactivity Argon, https://indico.cern.ch/event/765096/contributions/3295671/
190. Agnes P et al. *Phys. Lett. B* **743** 456 (2015); arXiv:1410.0653
191. Aalseth C E et al. *Eur. Phys. J. Plus* **133** 131 (2018)
192. Barbeau P S, Collar J I, Tench O *JCAP* **2007** (09) 009 (2007)
193. Scholz B J et al. *Phys. Rev. D* **94** 122003 (2016); arXiv:1608.03588
194. Ahlen S et al. *Phys. Lett. B* **195** 603 (1987)
195. Aalseth C E et al. (CoGeNT Collab.) *Phys. Rev. D* **88** 012002 (2013)
196. Davis J H, McCabe C, Boehm C *JCAP* **2014** (08) 014 (2014); arXiv:1405.0495
197. Derevianko A et al. *Phys. Rev. D* **82** 065006 (2010); arXiv:1007.1833
198. Aalseth C et al. *Phys. Rev. Lett.* **101** 251301 (2008); arXiv:0807.0879
199. Yue Q et al. (CDEX Collab.) *Phys. Rev. D* **90** 091701 (2014)
200. Yang L T et al. (CDEX Collab.) *Phys. Rev. Lett.* **123** 221301 (2019)
201. Ibe M et al. *J. High Energ. Phys.* **2018** (03) 194 (2018)
202. Liu Z Z et al. (CDEX Collab.) *Phys. Rev. Lett.* **123** 161301 (2019)
203. Jiang H et al. (CDEX Collab.) *Phys. Rev. Lett.* **120** 241301 (2018)
204. Liu S K et al. (CDEX Collab.) *Phys. Rev. D* **95** 052006 (2017)
205. Wang Y et al. (CDEX Collab.) *Phys. Rev. D* **101** 052003 (2020)
206. She Z et al. (CDEX Collab.) *Phys. Rev. Lett.* **124** 111301 (2020)
207. Aguilar-Arevalo A et al. (DAMIC Collab.) *Phys. Rev. D* **94** 082006 (2016); arXiv:1607.07410
208. Aguilar-Arevalo A et al. (DAMIC Collab.) *Phys. Rev. Lett.* **123** 181802 (2019); arXiv:1907.12628
209. Battaglieri M et al., arXiv:1707.04591
210. Luke P N et al. *Nucl. Instrum. Meth. Phys. Res. A* **289** 406 (1990)
211. Neganov B S, Trofimov V N, USSR Patent No. 1037771; *Otkryt. Izobret.* (146) 215 (1985)
212. Brink P L et al. *J. Phys. Conf. Ser.* **150** 012006 (2009)
213. Ahmed Z et al. (The CDMS II Collab.) *Science* **327** 1619 (2010)
214. Agnese R et al. (SuperCDMS Collab.) *Phys. Rev. Lett.* **120** 061802 (2018); arXiv:1708.08869
215. Agnese R et al. *Phys. Rev. Lett.* **121** 051301 (2018)
216. Agnese R et al. (The SuperCDMS Collab.) *Appl. Phys. Lett.* **103** 164105 (2013); arXiv:1305.2405
217. Agnese R et al. (CDMS Collab.) *Phys. Rev. Lett.* **111** 251301 (2013)
218. Agnese R et al. (SuperCDMS Collab.) *Phys. Rev. Lett.* **112** 241302 (2014); arXiv:1402.7137
219. Broniatowski A et al. (EDELWEISS Collab.) *Phys. Lett. B* **681** 305 (2009); arXiv:0905.0753

220. Armengaud E et al. (EDELWEISS Collab.) *Phys. Rev. D* **98** 082004 (2018); arXiv:1808.02340
221. Armengaud E et al. *JCAP* **2016** (05) 019 (2016); arXiv:1603.05120
222. Angloher G et al. *Astropart. Phys.* **23** 325 (2005); astro-ph/0408006
223. Willers M et al. *J. Phys. Conf. Ser.* **888** 012209 (2017)
224. Angloher G et al. *Eur. Phys. J. C* **76** 25 (2016); arXiv:1509.01515
225. Mancuso M et al. (The CRESST Collab.) *J. Low Temp. Phys.* **199** 547 (2020)
226. Amole C et al. (PICO Collab.) *EPJ Web Conf.* **95** 04020 (2015)
227. Behnke E et al. *Science* **319** 933 (2008); arXiv:0804.2886
228. Menéndez J, Gazit D, Schwenk A *Phys. Rev. D* **86** 103511 (2012)
229. Barnabé-Heider M et al. *Nucl. Instrum. Meth. Phys. Res. A* **555** 184 (2005); physics/0508098
230. Archambault S et al. *Phys. Lett. B* **711** 153 (2012); arXiv:1202.1240
231. Behnke E et al. (COUPP Collab.) *Phys. Rev. D* **86** 052001 (2012)
232. Amole C et al. (PICO Collab.) *Phys. Rev. Lett.* **114** 231302 (2015)
233. Amole C et al. (PICO Collab.) *Phys. Rev. Lett.* **118** 251301 (2017)
234. Crisler M B "PICO 250-liter Bubble Chamber Dark Matter Experiment", Presented at the SNOLAB Future Project Workshop, August 2013, https://www.snolab.ca/wp-content/uploads/2021/01/Crisler_PICO.pdf
235. Billard J, Mayet F, Santos D *JCAP* **2012** (07) 020 (2012)
236. Green A M, Morgan B *Astropart. Phys.* **27** 142 (2007)
237. Billard J, Mayet F, Santos D *JCAP* **2012** (04) 006 (2012)
238. Vahsen S E et al. *EAS Publ. Ser.* **53** 43 (2012); arXiv:1110.3401
239. Ahlen S et al. (DMTPC Collab.) *Phys. Lett. B* **695** 124 (2011)
240. Snowden-Ifft D P, Martoff C J, Burwell J M *Phys. Rev. D* **61** 101301 (2000); astro-ph/9904064
241. Santos D et al. *J. Phys. Conf. Ser.* **460** 012007 (2013)
242. Nakamura K et al. *J. Phys. Conf. Ser.* **375** 012013 (2012)
243. Aleksandrov A et al., arXiv:1604.04199
244. Caracciolo V et al. *J. Phys. Conf. Ser.* **718** 042011 (2016)
245. Directional Dark Matter Search. Directional WIMP detection with carbon nanotubes (DCaNT), http://web.infn.it/cygnus/dcant/
246. Nygren D R *J. Phys. Conf. Ser.* **460** 012006 (2013)
247. Charpak G et al. *Nucl. Instrum. Meth.* **62** 262 (1968)
248. Giomataris Y et al. *Nucl. Instrum. Meth. Phys. Res. A* **376** 29 (1996)
249. Sauli F *Nucl. Instrum. Meth. Phys. Res. A* **386** 531 (1997)
250. Klingenberg R (on behalf of the ATLAS Pixel Collab.) *Nucl. Instrum. Meth. Phys. Res. A* **579** 664 (2007)
251. Guillaudin O et al. *EAS Publ. Ser.* **53** 119 (2012); arXiv:1110.2042
252. Reinking G F, Christophorou L G, Hunter S R *J. Appl. Phys.* **60** 499 (1986)
253. Battat J B R et al. *Phys. Rep.* **662** 1 (2016); arXiv:1610.02396
254. Vahsen S E et al. *Nucl. Instrum. Meth. Phys. Res. A* **788** 95 (2015)
255. Yakabe R et al. *J. Phys. Conf. Ser.* **1342** 012082 (2020)
256. Snowden-Ifft D P, arXiv:1308.0354
257. Battat J B R et al. *Phys. Dark Universe* **9–10** 1 (2015)
258. Battat J B R et al. *JINST* **12** P10009 (2017); arXiv:1707.09431
259. Leyton M (on behalf of the DMTPC Collab) *J. Phys. Conf. Ser.* **718** 042035 (2016)
260. Deaconu C et al. *Phys. Rev. D* **95** 122002 (2017); arXiv:1705.05965
261. Battat J B R et al. *Astropart. Phys.* **91** 65 (2017); arXiv:1701.00171
262. Asada T et al. *Prog. Theor. Exp. Phys.* **2017** 063H01 (2017)
263. Umemoto A et al. *Prog. Theor. Exp. Phys.* **2019** 063H02 (2019)
264. Alexandrov A et al. *JINST* **10** P11006 (2015)
265. Alexandrov A et al. *JINST* **11** P06002 (2016)
266. Alexandrov A et al. *Sci. Rep.* **7** 7310 (2017)
267. Alexandrov A, De Lellis G, Tioukov V *Sci. Rep.* **9** 2870 (2019)
268. Alexandrov A et al. *Nucl. Instrum. Meth. Phys. Res. A* **824** 600 (2016)
269. Katsuragawa T et al. *JINST* **12** T04002 (2017)
270. Alexandrov A et al. *Sci. Rep.* **10** 18773 (2020)
271. De Lellis G et al., "Method and optical microscope for detecting particles having sub-diffractive size", Patent No. WO2018122814
272. Alexandrov A et al. *Astropart. Phys.* **80** 16 (2016); arXiv:1507.03532
273. Kimura M et al. *Nucl. Instrum. Meth. Phys. Res. A* **845** 373 (2017)
274. Golovatiuk A, De Lellis G, Ustyuzhanin A *J. Phys. Conf. Ser.* **1525** 012108 (2020)
275. Press Release of NEWSdm Experiment, http://news-dm.lngs.infn.it
276. Cappella F et al. *Eur. Phys. J. C* **73** 2276 (2013)
277. Capparelli L M et al. *Phys. Dark Universe* **9–10** 24 (2015)
278. Capparelli L M et al. *Phys. Dark Universe* **11** 79 (2016)
279. Nygren D R *J. Phys. Conf. Ser.* **460** 012006 (2013)
280. Cao H et al. (SCENE Collab.) *Phys. Rev. D* **91** 092007 (2015)
281. Ginzburg V L *Phys. Usp.* **42** 353 (1999); *Usp. Fiz. Nauk* **169** 419 (1999)